Nidovirus-Associated proliferative pneumonia in the green tree python (Morelia viridis)

Dervas, Eva ; Hepojoki, Jussi ; Laimbacher, Andrea ; Romero-Palomo, Fernando ; Jelinek, Christine ; Keller, Saskia ; Smura, Teemu ; Hepojoki, Satu ; Kipar, Anja ; Hetzel, Udo

Abstract: In 2014 we observed a noticeable increase in sudden deaths of green tree pythons (Morelia 28 viridis). Pathological examination revealed accumulation of mucoid material within airways and lung, associated with enlargement of the entire lung. We performed full necropsy and histological examination on affected green tree pythons from different breeders to characterise the pathogenesis of this "mucinous" pneumonia. By histology we could show a marked hyperplasia of the airway epithelium and of faveolar type II pneumocytes. Since routine microbiological tests failed to identify a causative agent, we studied lung samples of a few diseased snakes by next-generation sequencing (NGS). From the NGS data we could assemble a piece of RNA genome <85% identical to nidoviruses previously identified in ball pythons and Indian pythons. We then employed RT-PCR to demonstrate the presence of the novel nidovirus in all diseased snakes. To attempt virus isolation, we established primary cell cultures of Morelia viridis liver and brain, which we inoculated with lung homogenates of infected individuals. Ultrastructural examination of concentrated cell culture supernatants showed the presence of nidovirus particles, and subsequent NGS analysis yielded the full genome of the novel virus, Morelia viridis nidovirus (MVNV). We then generated an antibody against MVNV nucleoprotein, which we used alongside RNA in situ hybridisation to demonstrate viral antigen and RNA in the affected lungs. This suggests that in natural infection MVNV damages the respiratory tract epithelium which then results in epithelial hyperplasia, most likely as an exaggerated regenerative attempt in association with increased epithelial turnover.

DOI: https://doi.org/10.1128/JVI.00718-17

Nidovirus-Associated Proliferative Pneumonia in the Green Tree Python (*Morelia viridis*)

Eva Dervas[1], Jussi Hepojoki[1,2], Andrea Laimbacher[3], Fernando Romero-Palomo[1], Christine Jelinek[1], Saskia Keller[1], Teemu Smura[2], Satu Hepojoki[1], Anja Kipar[1*], Udo Hetzel[1]

[1]Institute of Veterinary Pathology, Vetsuisse Faculty, University of Zürich, Zürich, Switzerland

[2]University of Helsinki, Medicum, Department of Virology, Helsinki, Finland

[3]Institute of Virology, Vetsuisse Faculty, University of Zurich, Switzerland

Running title: *Morelia viridis* nidovirus

Corresponding author's address:

Institute of Veterinary Pathology

Vetsuisse Faculty

University of Zurich

Winterthurerstrasse 268

CH - 8057 Zurich

Switzerland

Phone: +41 44 6358552

E-mail: anja.kipar@uzh.ch

Abstract

In 2014 we observed a noticeable increase in sudden deaths of green tree pythons (*Morelia viridis*). Pathological examination revealed accumulation of mucoid material within airways and lung, associated with enlargement of the entire lung. We performed full necropsy and histological examination on 12 affected green tree pythons from 7 different breeders to characterise the pathogenesis of this "mucinous" pneumonia. By histology we could show a marked hyperplasia of the airway epithelium and of faveolar type II pneumocytes. Since routine microbiological tests failed to identify a causative agent, we studied lung samples of a few diseased snakes by next-generation sequencing (NGS). From the NGS data we could assemble a piece of RNA genome <85% identical to nidoviruses previously identified in ball pythons and Indian pythons. We then employed RT-PCR to demonstrate the presence of the novel nidovirus in all diseased snakes. To attempt virus isolation, we established primary cell cultures of *Morelia viridis* liver and brain, which we inoculated with lung homogenates of infected individuals. Ultrastructural examination of concentrated cell culture supernatants showed the presence of nidovirus particles, and subsequent NGS analysis yielded the full genome of the novel virus, Morelia viridis nidovirus (MVNV). We then generated an antibody against MVNV nucleoprotein, which we used alongside RNA *in situ* hybridisation to demonstrate viral antigen and RNA in the affected lungs. This suggests that in natural infection MVNV damages the respiratory tract epithelium which then results in epithelial hyperplasia, most likely as an exaggerated regenerative attempt in association with increased epithelial turnover.

Importance

Fairly recently novel nidoviruses associated with severe respiratory disease were identified in ball pythons and Indian pythons. Herein we report isolation and identification of a further nidovirus from green tree pythons (*Morelia viridis*) with fatal pneumonia. We thoroughly characterize the pathological changes in the infected individuals, and show that nidovirus infection is associated with marked epithelial proliferation in the respiratory tract. We speculate that this and the associated excess mucus production can lead to the animals' death, by inhibitingthe normal gas exchange in the lung. The virus was predominantly detected in the respiratory tract, which renders transmission via the respiratory route likely. Nidoviruses cause sudden outbreaks with high mortality in breeding collections, most affected snakes die without prior clinical signs. These findings, together with those of other groups, indicate that nidoviruses are a likely cause of severe pneumonia in pythons.

Introduction

The green tree python or Southern green python, *Morelia viridis* (Schlegel, 1872), is an oviparous boid constrictor snake with natural habitats in several Indonesian islands, Florida, Papua New Guinea and North Australia (1). Over the recent years large numbers of *M. viridis* have been exported from Indonesia to Europe and America (2), and they have become increasingly popular in both private and zoological collections (3, 4). So far, the knowledge on infectious diseases of *M. viridis* is sparse (5).

Recently, fatal pneumonias have been reported in two other python species, ball pythons (*Python regius*) (6) and Indian pythons (*Python molurus*) (7); infection with novel nidoviruses was found as the common denominator (8, 9). The described viruses are approximately equidistant from the two current genera, *Torovirus* and *Bafinivirus*, of the *Torovirinae* subfamily in the family *Coronaviridae*, order *Nidovirales* (8–15), in which they will likely form a novel genus (9).

The order *Nidovirales* comprises four families of complex positive-sense single-stranded RNA (ssRNA+) viruses, *Arteriviridae*, *Mesoniviridae*, *Roniviridae* and *Coronaviridae*, which are also distinguished by their genome size: roniviruses (~26 kb) and coronaviruses (26-33 kb) are known as "large nidoviruses" (16–18), arteriviruses as "small nidoviruses" (13–16 kb), and mesoniviruses with an intermediate genome size between the two (16, 17, 19, 20). While roniviruses and mesoniviruses are known to infect crustaceans and insects (19, 21), arteriviruses have been associated with an acute respiratory syndrome and abortion in pigs (porcine reproductive and respiratory syndrome virus, PRRSV) or a lethal haemorrhagic disease in non-human primates (simian haemorrhagic fever virus, SHFV) (22). The *Coronavirinae* subfamily of the *Coronaviridae* includes several pathogens of mammals (Feline coronavirus; transmissible gastroenteritis virus; Equine coronavirus, to mention a few), birds andfish, and has provided a steady supply of emerging threats to human health

over the past 15 years, including Severe Acute Respiratory Syndrome (SARS) and Middle-Eastern Respiratory Syndrome (MERS) (23). The members of the second subfamily of the *Coronaviridae, Torovirinae,* have so far not generated similar threats. They include bafiniviruses, which infect ray-finned fish and induce renal tubular necrosis and necrotising hepatitis (24), and toroviruses, which infect mammals (including humans, cattle, horses, and pigs) (10, 11, 25–27). Toroviruses have a tropism for epithelial cells, of both the respiratory and alimentary tract (28–30); in cattle, an association with pneumonia has been reported (30, 31). Toroviruses exhibit a unique morphology, the viral particles are kidney- and/or rod-shaped, with a tubular, torus-shaped ribonucleoprotein (RNP) enveloped by a membrane decorated with spikes composed of S protein (32). The RNP comprises the nucleoprotein (N protein) and the ssRNA+ genome (33, 34).

In 2014, a Swiss breeder submitted two adult green tree pythons for diagnostic post mortem examination. Both animals had died with signs of a "mucinous" pneumonia. In the following year, the same breeder submitted another two individuals. These, as well as a further five green tree pythons from three additional breeders, all exhibited similar pathological findings. In 2016, additional cases were observed, involving two more breeding collections. As all routine diagnostic tests undertaken failed to identify potential causative viruses or specific bacterial agents, we initiated an investigation into the cause of this apparently emerging disease of green tree pythons.

Material and Methods

Animals. The study was performed on sixteen green tree pythons (*Morelia viridis*) from six breeding collections in Switzerland and one collection in Germany (Table 1). The collections varied in both size (i.e. number of breeding animals) and species range, from a single snake up to a collection of 50 snakes of various species.

All animals were submitted to the Institute of Veterinary Pathology, Vetsuisse Faculty, University of Zurich, for diagnostic purposes. Fifteen snakes had died spontaneously, one was euthanized following an ASPA (Animals Scientific Procedures Act 1986) schedule 1 (appropriate methods of humane killing, http://www.legislation.gov.uk/ukpga/1986/14/schedule/1) procedure. In each case, a full diagnostic post mortem examination was performed with owner's consent. For these diagnostic-motivated necropsies, no ethical permission is required at the University of Zurich.

The initial study population is represented by nine snakes, of which four (A1-A4) were from one breeder (A), each two from a second and third breeder (B1, B2 and C1, C2), and one (D1) from a fourth breeder (Table 1A). These animals were submitted between September 2014 and November 2015. After completion of the next-generation sequencing (NGS) study, another seven snakes were submitted (E1, F1, G1-G5) by another three breeders (E, F, G). All initial and another three snakes of the second cohort exhibited one common gross feature: the airways contained a variable amount of mucoid material which was most abundant in the faveolar lumen (Table 1A). The remaining four snakes (G2-G5) did not show any changes in the airways or lungs (Table 1B) and later served as controls.

Sample collection and screening for infectious agents. During post mortem examinations samples from all organs were collected and fixed in 10% buffered formalin for histological examination. Additional samples from brain, lung, liver, and kidney were stored at -80 °C for further analysis. Also, lung samples from the freshly euthanized snake (A2) and from two snakes that were necropsied within a few hours after death (B1, D1) were fixed in glutaraldehyde/paraformaldehyde and processed for transmission electron microscopy (TEM) as described (35).

Prior to performing NGS, six of the initial cases were screened for infectious agents: bacterial cultivation was attempted from the lungs of three snakes (A1, A3, D1) at the Institute of

139 Veterinary Bacteriology, Vetsuisse Faculty, University of Zurich; and lung samples from
140 another three snakes (B1, B2, C1) were submitted to a commercial lab (LABOKLIN, Basel,
141 Switzerland) for virus diagnostics (reovirus, paramyxovirus, Sunshine virus, nidovirus) (Table
142 1).

143 **Virus isolation and ultrastructural characterisation.** Primary tissue cultures of *Morelia*
144 *viridis* were established as described (35), using brain and liver material from a foetus (from a
145 clutch of B1 and B2). The tissue was trimmed into blocks (1 mm) and suspended in 5 ml of
146 minimal essential medium (MEM, ThermoFisher, Scientific, GIBCO) supplemented with
147 HEPES (25 mM), 10% fetal bovine serum (FBS; Biochrom), Gentamycin (0.05 mg/ml), L-
148 Glutamine (2 mM, Biochrom), 10% Tryptose Phosphate-Broth (DIFCO), and 20 µl α-D-
149 Glucose (90 g/l PBS) in sterile cell culture dishes (5 cm in diameter), and incubated at 30 °C
150 and 5% CO_2. Primary *Boa constrictor* lung (V/4Lu) and brain (V/4Br) cell lines were
151 established similarly as described above.

152 Cell cultures were used for inoculations at passage 8-15 (*M. viridis* cell lines), 30-35 for
153 V/4Lu and V/4Br. Briefly, after initial trimming of lungs into blocks (>1 mm) the pieces were
154 mechanically homogenized in 1 ml of Trypsin-EDTA solution (0.25%, Gibco, Thermo Fisher
155 Scientific), the cell debris pelleted by centrifugation (5 min at 1,000 x g), and the remaining
156 supernatant was diluted in 5 ml of MEM supplemented with 25 mM HEPES (Thermo Fisher
157 Scientific) and 15% FBS (Biochrom), and 0.45 µm filtered. One ml of the filtered lung
158 homogenate further diluted 1:10 in growth medium was used to inoculate 75-cm^2 flasks of
159 both brain and liver cells. The medium was changed at 1-2 day intervals until most cells
160 detached or died. The supernatants were frozen at -20 °C, pooled, and 0.45 µm filtered. The
161 cleared supernatant was loaded onto a cushion of 30% (w/v) sucrose in PBS, concentrated at
162 100,000 g for 2 h at 4 °C and solubilized in PBS. For protection, protease inhibitor (Protease
163 inhibitor cocktail tablets complete, Mini, EDTA-free, Roche Diagnostics, Mannheim,

Germany) was added to the supernatant. For negative staining, samples were adsorbed to carbon-coated parlodion films mounted on 300 mesh/inch copper grids (EMS, Fort Washington, PA, USA) for 10 min, washed once with H_2O, and stained with 2% phosphotungstic acid (PTA), pH 7.0 (Aldrich, Steinheim, Germany) for 1 min. Specimens were analyzed in a transmission electron microscope (CM12, Philips, Eindhoven, The Netherlands) equipped with a CCD camera (Ultrascan 1000, Gatan, Pleasanton, CA, USA) at an acceleration voltage of 100 kV.

M. viridis brain and liver cells were harvested at 3, 4, and 5 days post infection (dpi) and pelleted by centrifugation at 5,000 rpm for 5 min at room temperature (Eppendorf centrifuge 5415C, NIST). The pellets were fixed with 2.5% glutaraldehyde in PBS (pH 7.4), and routinely resin embedded for TEM (35). To obtain a retrovirus-free virus preparation, the supernatant collected from *M. viridis* liver cell cultures inoculated with lung homogenate was used to inoculate a *B. constrictor* kidney cell line I/1Ki (35). Supernatant was collected from the infected I/1Ki cells at two day intervals until 8 dpi. The supernatants were filtered through a 0.45 µm filter, pooled, aliquoted, and stored at -80 °C.

Next-generation sequencing (NGS). RNA was isolated from the lungs of three diseased snakes (animals A2, B1, D1, Table 1) with TRIzol® reagent (Life Technologies) according to the manufacturer's protocol, using 5 µg of RNA grade glycogen (ThermoFisher Scientific) as carrier. The RNA samples were initially treated with DNAse I (Fermentas), followed by re-purification with the GeneJET RNA purification kit (Thermo Fisher Scientific). Ribo-Zero Gold rRNA Removal Kit for Epidemiology (Illumina) was used according to the manufacturer's protocol to further clean the RNA. In the case of virus sequencing from cell culture supernatants, the RNA isolation was done using QIAamp Viral RNA Mini Kit (QIAGEN) following the manufacturer's protocol without addition of carrier RNA. For RNA

189 isolated from cell culture supernatants, the rRNA was removed with NEBNext rRNA
190 Depletion Kit (New England Biolabs). The indexing and NGS library preparation was
191 accomplished with the NEBNext Ultra RNA Library Preparation Kit (New England Biolabs)
192 according to the manufacturer's protocol. The libraries were quantified using the NEBNext
193 Library Quant Kit for Illumina (New England Biolabs). Pooled libraries were sequenced on
194 an Illumina MiSeq (Illumina) using the MiSeq Reagent Kit v3 (Illumina), with 291-bp (for
195 lung samples) and 300-bp (for RNA isolated from cell culture supernatant) reads from both
196 ends (paired-end). *De novo* sequence assembly was performed after removing reads matching
197 to the host genome, both with MIRA version 4.9.5. (http://mira-assembler.sourceforge.net/)
198 on CSC (IT Center for Science Ltd., Finland) Taito supercluster. The generated contiguous
199 sequences (contigs) from the lung sample run were initially screened by nucleotide BLAST
200 (blastn, at https://blast.ncbi.nlm.nih.gov/Blast.cgi) and several contigs matching ball python
201 nidovirus (BPNV; NCBI Reference Sequence NC_024709.1) and Python nidovirus (PNV;
202 GenBank accession KJ935003.1) were identified. In attempt to obtain full-length genome the
203 contigs were mapped to BPNV and PNV genomes using the BWA-SW tool (36) in Unipro
204 UGENE (37). However, contig with almost full-length genome for a novel nidovirus
205 subsequently named "Morelia viridis nidovirus (MVNV)" was obtained via *de novo* assembly
206 from RNA isolated from cell culture supernatant. The genome open reading frames, ORFs,
207 were detected using Unipro UGENE. The contig coverage was determined using Bowtie2
208 reference alignment of the entire NGS data in Unipro UGENE.

209 **Phylogenetic analysis and bioinformatics.** Since Blastn search of the contig obtained by *de*
210 *novo* assembly from purified virus material suggested that python nidoviruses (BPNV, PNV,
211 a proposed new genus in the *Torovirinae* sub-family of nidoviruses) were the most
212 homologous group to MVNV, representative sequences of this sub-family (i.e. genus
213 *Torovirus*, *Bafinivirus* and python nidoviruses) were downloaded from the GenBank. The
214 amino acid sequences of the conserved ORF1b were aligned using ClustalW algorithm

implemented in MEGA version 6.06 (38) followed by manual refinement. The best-fit substitution model was sought using maximum likelihood method implemented in MEGA 6.06. Phylogenetic trees were constructed using the Bayesian Monte Carlo Markov Chain (MCMC) method implemented in BEAST version 1.8.0 (39). The analyses were performed with LG+G+I model of substitution, strict clock and constant size demographic model. The Bayesian analyses were run for 10 million states and sampled every 1000 states. The analyses were carried out on CSC – IT Center for Science Ltd. (Espoo, Finland). Posterior probabilities were calculated with a burn-in of 1 million states and checked for convergence using Tracer version 1.6 (40). The mfold Web Server (available at http://unafold.rna.albany.edu/?q=mfold) was utilized for determining the RNA folding (41) around the ribosomal frameshift signal (RFS). Unipro UGENE (37) was utilized for nucleotide alignments (MUSCLE (42)) around the RFS. HMMER: biosequence analysis using profile hidden Markov models (available at http://hmmer.org/, (43) was used to identify conserved domains in the identified ORFs.

Quantitative reverse transcription-polymerase chain reaction (qRT-PCR). RNA was extracted from lung tissue samples with the TRIzol® reagent (Life Technologies) utilizing mechanical homogenization with a MagNA Lyser (Roche). After addition of chloroform and separation of the RNA-containing phase by centrifugation (15 min, 12,000 x g, 4°C) the RNA was purified with the QiaGEN RNeasy Mini Kit (Qiagen) following the manufacturer's protocol for RNA clean up.

The amount of RNA in the samples was measured by Nanodrop 2000c (Thermo Fisher Scientific), and the samples were subsequently diluted with RNase-free water to a concentration of 150 ng/µl to allow comparative assessment.

A Taqman qRT-PCR assay was set up using the following primers (Microsynth AG, Switzerland): Nido-fwd, 5´-AGTCATCTGTCTCGACCACCT-3´ and Nido-rev, 5´-ACATGTAGAGCACTTTGACTGGTT-3´. The sequence for the probe (Microsynth AG, Switzerland) was: Nido-probe, FAM-CGACAACTGGGTCATCAGACGC-TAMRA.

241 The qRT-PCR was performed on an Applied Biosystems 7500 fast Real-Time PCR system
242 using 96-well plates. The reaction volume (25 µl) consisted of 12.5 µl of One step qRT-PCR
243 MasterMix (Eurogentec), each 1 µl of forward and reverse primer (10 µM), 1 µl of probe (10
244 µM), 0.125 µl of reverse transcriptase (Euroscript RT and RNase Inhibitor Mix, Eurogentec),
245 5 µl (750 ng) of template RNA, and 4.5 µl of DEPC-treated H_2O.
246 The qRT-PCR was set up with the following cycling conditions: 1) 30 min at 48 °C, 2) 10
247 min at 95 °C, 3) 15 s at 95 °C, and 4) 1 min at 60 °C, 40 cycles between steps 3 and 4. The
248 data was collected during step 4 of the RT-PCR programme.
249 **Recombinant protein expression and generation of anti-MVNV nucleoprotein (N**
250 **protein) antiserum.** To identify the ORF for the N protein gene in the genome of the novel
251 virus isolate, the *de novo* assembled genome was aligned with BPNV (NCBI Reference
252 Sequence NC_024709.1) and PNV (GenBank accession KJ935003.1) genomes using
253 MUSCLE (42) in Unipro UGENE (37). The N protein coding region was obtained from
254 cDNA transcribed with random primers using RNA isolated from supernatants of cultured
255 cells inoculated with lung tissue homogenate (see above). The cDNA transcription was done
256 using RevertAid Transcriptase (ThermoFisher Scientific) following the protocol for random
257 hexamer amplification. The PCR amplification of the whole N protein coding region was
258 done with primers designed according to the Champion pET Directional TOPO Expression
259 Kit's manual (ThermoFisher Scientific) using Phusion Flash High-Fidelity PCR Master Mix
260 (ThermoFisher Scientific). The PCR product was purified from agarose gel using GeneJET
261 Gel Extraction Kit (ThermoFisher Scientific) and ligated to pET101/D-TOPO vector with N-
262 terminal V5-epitope and His-tags (ThermoFisher Scientific). The ligated vector was
263 transformed to One Shot TOP10 Competent Cells (ThermoFisher Scientific) and clones with
264 the desired insert were screened by plating on Luria Broth (LB) agar plates with 100 µg/ml
265 ampicillin. Individual colonies were grown in 5 ml of LB supplemented with 100 µg/ml
266 ampicillin overnight and the plasmids purified using the GeneJET Plasmid Miniprep Kit

(ThermoFisher Scientific) following the manufacturer's recommendation. The plasmids were sequenced (Microsynth AG, Switzerland), using T7 forward and reverse primers. The N protein containing plasmid was transformed into BL21 Star (DE3) One Shot Chemically Competent E. coli (ThermoFisher Scientific), and protein expression was done in LB supplemented with 100 μg/ml carbenicillin (Sigma-Aldrich) and 1% glucose (Sigma-Aldrich) according to the manufacturer's recommendation. The recombinant N protein expressed in inclusion bodies was purified using Chelating Sepharose Fast Flow (GE Healthcare Life Sciences) with cobalt as the immobilized metal ion and 8M urea in all buffers. The protein in the elution buffer (50 mM Tris, 500 mM NaCl, 300 mM imidazole, 8M Urea, pH 7.5) was concentrated using a 10 kDa cut off Amicon Ultra-15 Centrifugal Filter Unit (EMD Millipore), and buffer exchange (to 25 mM Tris, 75 mM NaCl, pH 7.5) was achieved by decreasing the urea concentration slowly using Slide-A-Lyzer Dialysis Cassette 3.5 MWCO (ThermoFisher Scientific). The purified recombinant protein was used to immunize a rabbit applying the following scheme: initial immunization (day 0), first booster (day 7), second booster (day 14), third booster (day 42), and final bleeding (day 49) (BioGenes GmbH, Berlin, Germany). The generated antiserum was cleaned by affinity purification similarly to previous descriptions (44, 45). Briefly, 500 μg of purified recombinant N protein was dialyzed in PBS followed by coupling to CnBr-activated Sepharose 4B (GE Healthcare) following manufacturer's protocol. The affinity matrix was packed into Econo-Pac Chromatography columns (Bio-Rad) and antiserum was passed through the column by gravity flow. After washing with several column volumes of PBS, the bound antibodies were eluted with 0.1M glycine (pH 2.5) and the fractions were neutralized by addition of 1M Tris, pH 8.5. The affinity purified antibody was dialyzed against PBS, and concentrated using 10 kDa cut off Amicon Ultra-15 Centrifugal Filter Unit (EMD Millipore). The purified antibody was mixed with glycerol (50%) and stored in aliquots at -20 °C.

Immunofluorescence staining, qRT-PCR of cell culture supernatants, and estimation of virus titer.

For immunofluorescence staining *M. viridis* (brain) and *B. constrictor* (kidney, lung, brain) cells were detached by trypsin, washed with growth medium, and seeded on glass bottom 24-well plates (IBL, Gerasdorf, Austria). The attached cells were inoculated by incubation with 250 µl of 1/10 diluted (in growth medium) MVNV isolated on I/1Ki. After 1 h incubation at 30 °C the cells were washed twice with supplemented growth medium, and finally 1 ml of supplemented growth medium was added to each well. For each cell line three wells were inoculated with MVNV and three wells were mock-infected with supplemented growth medium. At 3 dpi the cells were fixed by replacing the supplemented growth medium with 4% EM-grade paraformaldehyde in PBS followed by 15 min incubation at RT. After fixation the cells were washed once with PBS, permeabilised (0.25% Triton X-100 and 3% BSA in PBS), and left in PBS until staining. The replicate wells (3 replicates of MVNV and mock-infected for each cell line) were incubated with anti-MVNV NP antibody at 1:1,000, 1:2,000, or 1:4,000 dilution (in PBS) for 1 h at RT, washed 5 times with PBS, incubated 45 min at RT with 1:1000 PBS-diluted AlexaFluor 594 labelled goat anti-rabbit secondary antibody (Invitrogen), washed 4 times with PBS, incubated for 1 min with DAPI in PBS, washed twice with dH_2O, air dried, and coverslipped with FluoreGuard mounting medium (Biosystems, Switzerland). The images of MVNV- and mock-infected cells were taken at a 400 x magnification with a Nikon Eclipse Ti-U inverted microscope with NIS Advanced Research software, 1:2,000 diluted anti-MVNV NP antiserum yielded the best signal to noise ratio.

For monitoring virus production cell culture supernatant was collected at 0, 1, 2, and 3 dpi. At each time point 47 µl from each well was collected and samples from replicate wells were pooled to make ~140 µl. The samples were stored frozen at -20 °C prior to RNA isolation with QIAamp Viral RNA Mini Kit (QIAGEN). The cell culture supernatants were analysed

by qRT-PCR in duplicates, and the relative amount of virus RNA (as compared to 0 dpi) at each time point was determined using $2^{-\Delta Ct}$.

To estimate the virus titer in MVNV stock isolated on *B. constrictor* kidney cell line (I/1Ki), *M. viridis* brain cells were trypsinised, washed with supplemented growth medium, and seeded onto 96-well tissue culture plate (TPP, Switzerland) in 135 µl of supplemented growth medium per well. A serial 10-fold dilution of MVNV stock was prepared reaching $1{:}10^6$ dilution, and 15 µl of each dilution was pipetted on 12 parallel wells. The plate was incubated for 5 d at 30 °C (until a clear cytopathic effect, CPE, was seen in all wells inoculated with MVNV dilutions).

Histology, immunohistology and RNA-in situ hybridisation. Formalin-fixed tissue samples were trimmed and routinely paraffin wax embedded. Sections (4-5 µm) were prepared and stained with haematoxylin and eosin (HE) and the PAS/Alcian Blue stain for the evaluation of mucus-producing cells, or used for immunohistology (IH) and RNA-in situ hybridisation (RNA-ISH) (performed on the lungs of all affected snakes, plus all major organs/tissues of five affected animals (B1, B2, A4, G1, E1) and one healthy individual (G5)).

IH was performed to demonstrate nidovirus NP in tissue sections, using the custom made rabbit polyclonal antibody (see above). The EnVision HRP detection system (Dako, Baar, Switzerland) was applied. After deparaffination, sections were incubated in peroxidase-blocking solution (Dako) for 10 min at room temperature to block any endogenous peroxidase activity, followed by incubation with the primary antibody (anti-MVNV N protein; diluted 1:1,000 in Dako dilution buffer) for 12-15 h at 4°C. This was followed by incubation with Envision + System HRP Rabbit Antibody (Dako) according to the manufacturer's protocol. The reaction was visualised with diaminobenzidintetrahydrochloride (DAB), followed by counterstaining with haematoxylin. The sections underwent a TBS-Tween wash (Tris-buffered saline solution containing Tween 20, pH 7.6) for 10 min between each incubation

342 step. A formalin-fixed, paraffin embedded cell pellet prepared from the infected cell cultures
343 served as positive control. Consecutive sections incubated with the pre-immune serum instead
344 of the specific primary antibody served as negative controls.

345 Sections from lungs and trachea were also stained by IH for cytokeratins (clone PCK-26,
346 Novus Biologicals) to highlight respiratory and epithelial cells, for cleaved caspase-3 (rabbit
347 anti-human cleaved caspase-3 monoclonal antibody, Asp175, clone 5A1E; Cell Signaling
348 Technology) to demonstrate apoptotic cells, and for proliferating cell nuclear antigen (mouse
349 anti-rat PCNA, clone PC10; Dako) to detect proliferating cells, using routine protocols
350 established for other species (46–48). Intestinal epithelium was used as a positive control for
351 all three detection systems after cross reactivity of the antibodies was confirmed by a
352 comparison of the expression pattern in the python with those seen in the respective
353 mammalian tissues.

354 For RNA-ISH, the RNAscope technology (Advanced Cell Diagnostics Inc., Newark, USA)
355 was employed, using a set of 30 Z-oligoprobes (based on the MVNV genome) and following
356 the manufacturer's instructions (49). DAB was used as the chromogen and haematoxylin for
357 counterstaining. A formalin-fixed, paraffin embedded pellet of virus infected cells served as
358 positive control. *DapB* (the bacterial gene coding for dihydrodipicolinate reductase) was used
359 as a negative control. RNA preservation was confirmed by the detection of a housekeeping
360 gene, ubiquitin C (*UBC*).

361 **Morphometry.** The quantitative assessment of the observed changes in the (respiratory)
362 epithelium was undertaken in the proximal, bronchial lung, as the caudal part is non-
363 respiratory and taken up by the air sacs Three regions were defined in the proximal, bronchial
364 lung, based on their epithelial cover and functions (Fig. 9; Fig. 2A): 1) The luminal part of the
365 primary trabeculae: This is covered by multilayered pseudostratified "bronchial-type"
366 epithelium, dominated by ciliated cells, with few secretory and goblet cells, supported by a

thick smooth muscle layer (i.e. myoelastic bundles) (50, 51). 2) Middle level and 3) base of the faveolae: The faveolae are covered by a single-layered epithelium similar to that in the mammalian lung ("gas exchange epithelium"), dominated by flat type I pneumocytes with thin, cytoplasmic extensions that cover the pulmonary capillaries and contain micropinocytotic vesicles (52). Between the capillaries lie the surfactant producing type II pneumocytes, cuboidal cells with short microvilli that contain lamellar bodies and numerous micropinocytotic vesicles (53). In addition, so-called "secretory cells" containing secretory granules have been described (50).

HE- and cytokeratin-stained cross-sections of the lungs were examined and photographed using a light microscope (Eclipse Ni-U, Nikon Corp.), and the images analysed with the associated imaging software (NIS-Elements AR, Nikon Corp.).

The average total height of the epithelial layer was determined in each of the three regions. For this purpose, the distance between the apical epithelial cell border and the basal membrane was measured at each 10 points over three 300 µm wide epithelial segments in each region in the cytokeratin stained section at a 200-fold magnification (Fig. 9B, D, E). For each location, the average value obtained for each of the three segments was used to determine the average height.

As we also observed an apparent increase in the cell layers of the generally multilayered epithelium in several diseased animals in region 1 and saw evidence of increased cellularity in the other two regions, we counted the total number of epithelial cell nuclei in each three 200 µm segments in all three regions in the cytokeratin stained section at a 400-fold magnification (Fig. 9C).

Statistical Analysis. Statistical analyses were performed to assess the epithelial thickness and cellularity, using SPSS Statistics 17.0.0 (IBM), a 0.05 significance level was utilized for all calculations. A Mann-Whitney U test for independent samples (t-test) was applied to compare lung parameters between non-infected and infected snakes.

Accession number(s).

MVNV genome is available in GenBank under accession number MF351889 and the raw NGS data is available at http://www.ncbi.nlm.nih.gov/biosample/7248312.

Results

Animals, clinical signs, macroscopical and histological features and results of screening for infectious agents. In 2014-2016, multiple *Morelia viridis* affected by a similar disease arrived for post mortem examination: four from one breeder (A1 and A2 in 2014, A3 and A4 in 2015), five from three additional breeders (B1, B2, C1, C2, and D1 in 2015), and three animals from three additional breeding collections (E1, F1, and G1 in 2016). Of these 12 snakes, four had died suddenly without any obvious clinical signs and seven had exhibited respiratory distress and expulsion of mucus for a period of a few hours to more than one week before death; for one animal no clinical history was available. All animals were adult, ranging from 1 to 8 years of age (Table 1A). Six snakes were female, six male. Upon gross post mortem examination all snakes exhibited a variable amount of mucoid material in the airways and, most abundant, in the faveolar spaces of the lung. In some animals, the entire trachea, the internal choanae and the caudal air sacs were obliterated by mucoid material (Fig. 1), and the lung parenchyma appeared thickened. The histological examination revealed a variable degree of epithelial thickening in trachea and lung and a mild to moderate interstitial lymphoplasmacellular and heterophilic infiltration of the lung parenchyma (Fig. 2). In one animal (E1) a moderate multifocal granulomatous-necrotising nephritis was additionally

observed. The four control snakes (G2-6), i.e. animals that had been euthanized due to non-respiratory diseases (Table 1B), did not exhibit similar gross and/or histological changes (Fig. 2).

We suspected an infectious cause and had routine bacteriological examinations performed on the lungs of selected snakes from the 2014 and 2015 cohort (A1, A3, D1). This only yielded a non-specific bacterial flora (i.e. no primary pathogens; *Pseudomonas aeruginosa, Proteus sp., Citrobacter braakii*, *Achromobacter xylosoxidans, Stenotrophomonas maltophilia* and *Providencia rettgeri*). A further three animals, from the 2015 cohort (B1, B2, C1) were then screened in a commercial laboratory for a range of potentially pathogenic viruses (i.e. reovirus, paramyxovirus, Sunshine virus, nidovirus); these tests yielded negative results.

Virus isolation in tissue cultures. As the routine bacteriological and virological tests failed to identify a common denominator for the diseased snakes, we decided to attempt virus isolation. For this purpose we prepared primary cell cultures of green tree python fetal liver and brain (Fig. 3A). After four passages the cells began to proliferate more rapidly and we could expand the cultures enough to attempt isolation of the unknown pathogen. When we used lung homogenates from diseased snakes (Table 1A) to inoculate both cultures, we observed the first evidence of a cytopathic effect (enlargement, rounding, and cytoplasmic vacuolisation of cells) and loss of adherence (Fig. 3B) at approximately 3 dpi. At 6 dpi almost the entire monolayer was affected and most cells had rounded and/or detached. (Fig. 3C). The ultrastructural examination of a cell pellet prepared from the cultures at 1 dpi identified abundant tubular viral structures arranged in stacks within the cytoplasm of infected cells (Fig. 3D, E). We concentrated the supernatants of the infected cells by ultracentrifugation and examined the pelleted material by TEM under negative staining. TEM analysis demonstrated rod- and kidney-shaped virions of approximately 120 nm length (Fig. 3F), consistent with torovirus particles (29, 54).

Identification of nidovirus by NGS and confirmation of the findings by real-time RT-PCR. In parallel to our attempts at virus isolation, we decided to employ NGS for the identification of the causative agent(s) for the pneumonia. We isolated RNA from lung homogenates of three animals (A2, B1, D1) and performed RNA sequencing. For two snakes (B1, D1) only contigs matching bacterial genomes were identified. We interpreted these bacterial sequences to most likely represent either contamination during post mortem sample collection or, more likely, secondary bacterial infection, as both had also shown moderate diffuse heterophil infiltration in the lung. From the third snake (A2), however, we obtained a single ~21.000 nt contig and several shorter contigs matching the previously identified "Ball python nidovirus (BPNV)" and "Python nidovirus (PNV)" (~85% identical to both) (9, 8). In total we obtained ~28.000 nt (~75-80%) of the genome from the lung sample. In addition to the novel nidovirus isolate, we identified a contig matching endogenous retrovirus genes with very high coverage, which we describe in a separate report (Hepojoki et al., in preparation). However, the retrovirus was also present in the supernatants of *M. viridis* cell cultures inoculated with lung homogenate. We decided to attempt producing a nidovirus preparation devoid of the contaminating retrovirus. To do this we inoculated boid kidney cells with supernatant collected from *Morelia viridis* liver cell culture inoculated with lung homogenates, since Huder et al. previously reported species-restricted growth of an endogenous python retrovirus (55). Using this approach we obtained a pure nidovirus isolate as confirmed by retrovirus-specific RT-PCR. We then performed end-point titration to quantify the number of infectious units in the MVNV stock on *M. viridis* brain cells, and could detect $2.25*10^{10}$ focus forming units per 1 ml of cell culture supernatant. RNA extracted from the pure nidovirus preparation was subjected to another NGS run, which yielded almost a full-length genome in a single contig. We then performed a reference assembly using BPNV as the template to recover the missing (some 150 nt in total) genome

ends for the novel virus, Morelia viridis nidovirus (MVNV). The overall genome structure of MVNV (GenBank accession number MF351889) was similar to that of BPNV and PNV (Fig. 4A). The identified contig contains eight partially overlapping open reading frames, ORFs, flanked by 5'UTR (~650 nt) and 3'UTR (~920 nt). We used HMMER3 to look for functional domains in the detected ORFs, and collected domains detected at high probability in Table 2. We also identified a putative ribosomal frameshift signal (RFS) sequence near the end of ORF1a. To further study the RFS, we aligned the sequences of other nidoviruses identified in snakes around the RFS and used mFOLD to predict the structure around this region in MVNV genome (Fig. 4B). The NGS data (raw data available at http://www.ncbi.nlm.nih.gov/biosample/7248312), coverage for MVNV genome is shown in Fig. 4C. The nt and amino acid identities between the novel nidovirus isolate and other python nidoviruses are indicated in Table 3.

We then tested whether the isolated MVNV could infect other cell lines. For this purpose we selected brain, kidney and lung cell lines of *B. constrictor*, and used *M. viridis* brain cells as the positive control. We also designed a Taqman real-time RT-PCR to be able to quantify and monitor nidovirus RNA in cell culture supernatants and lung tissue samples of the diseased snakes. Analysis of the cell culture supernatants collected from different cell lines inoculated with MVNV showed clear amplification in *B. constrictor* kidney and lung cells (Fig. 4D). The cytopathic effect on *M. viridis* brain cells was extremely severe, and therefore similar quantification could not be performed. The infected cells were stained using anti-MVNV NP antiserum at 3 dpi and all cell lines, except *B. constrictor* brain (only few infected cells were detected), showed to be extremely permissive for MVNV (Fig. 5).

As ORF1b is the most conserved ORF among nidoviruses (17), we selected this region for the phylogenetic analysis. The phylogenetic tree suggests that MVNV forms anoutgroup to BPNV and PNV (Fig. 6). Further, the python nidoviruses cluster together with Shingleback nidovirus (KX184715) (56), Xinzhou nematode virus 6 (KX883637), Xinzhou toro-like virus

493 (NC_033700), and bovine nidovirus (NC_027199) (31). Consistent with the previous reports,
494 these form a clade that is separate from both the genus Bafinivirus and the genus Torovirus
495 (Fig. 6).
496 Finally, we used RNA isolated from cell cultures inoculated with lung homogenates of an
497 infected snake as the positive and RNA isolated from a *Boa constrictor* as the negative
498 control in the real-time RT-PCR. All diseased snakes were tested positive for nidovirus RNA
499 in the lungs. In contrast, the four snakes without gross and/or histological evidence of
500 pneumonia were negative.
501
502 **Nidoviruses are associated with pneumonia in *M. viridis***. The histological examination
503 confirmed that all diseased snakes had suffered from a chronic pneumonia with epithelial
504 thickening in trachea and lung (Fig. 2) and excess mucus in the lumen of lungs and airway.
505 The inflammatory component was represented by mild to moderate multifocal interstitial
506 infiltration of lymphocytes, plasma cells and/or heterophils (Fig. 2E). The mucus filling the
507 faveolar space often contained heterophils and cell debris. In three of the nine tracheas
508 examined, we also observed a variable degree of mixed infiltration (heterophils, macrophages,
509 lymphocytes). Over its entire length, the lung epithelium exhibited numerous epithelial cells
510 that contained mucus as indicated by the PAS-Alcian Blue staining (Fig. 7A, C, E). In region
511 1, at the trabeculae, the mucus containing cells had the ultrastructural features of secretory
512 cells (50) (Fig. 7B). In regions 2 and 3 (faveolar epithelium), where the increase of these cells
513 was most striking, they exhibited the morphology of type II pneumocytes (Fig. 7D, F) (51);
514 their number varied in affected snakes and ranged from occasional patchy aggregates to
515 diffuse lining of the entire faveolae, associated with an almost complete absence of type I
516 pneumocytes (Fig. 2E). Ultrastructurally, these cells exhibited serous/mucous granules instead
517 of the lamellar bodies that are characteristic for type II pneumocytes (Fig. 7B, D, F); they
518 have recently been described as “transformed” type II pneumocytes (58).

519 Having detected nidoviral RNA in the affected lungs, we aimed to identify the viral target
520 cells. For this purpose, we employed both RNA-ISH and IH. Viral RNA and antigen (N
521 protein) were detected in the cytoplasm of the trabecular pseudostratified epithelium (region
522 1) and of both type I and type II pneumocytes lining the faveolar space (regions 2 and 3) in all
523 affected snakes (Fig. 8A-D). Intact and degenerated cells shed into the mucus were found to
524 be infected, and occasionally we also detected cell-free viral RNA and antigen (Fig. 8B).
525 Infected cells varied in number between animals and in individual snakes also in different
526 areas of the lung. In the hyperplastic epithelium of region 1, most cells exhibited a weak,
527 focal cytoplasmic reaction, and only the superficial cell layer contained abundant viral antigen
528 (Fig. 8B). The new type II pneumocytes that seemed to progressively replace the type I cells
529 exhibited a similarly weak focal reaction, whereas the fully differentiated pneumocytes were
530 strongly positive for viral antigen (Fig. 8C, D), suggesting more efficient virus replication.
531 When examined, the trachea (n=9) and the nasopharyngeal epithelium (n=1) also exhibited
532 infected, degenerating epithelial cells (Fig. 8E, F). Viral antigen was detected in few epithelial
533 cells of the oesophagus in one animal with acute pneumonia (G1). Interestingly, viral antigen
534 was also detected cell-free and in a few macrophages in the focal granulomatous-necrotising
535 nephritis in another affected animal (E1). We did not detect viral RNA or antigen in other
536 tissues ofthe infected snakes including stomach and intestines, or in the lungs of the control
537 snakes (G2-6).
538 We could demonstrate cytoplasmic accumulations of tubular structures, ranging from 150 nm
539 to 250 nm in length in rare epithelial cells with the morphology of type II pneumocytes by
540 ultrastructural examination (Fig. 8G).
541 The epithelial thickening was the most striking feature in the lungs of the nidovirus-positive
542 snakes. We therefore performed a more detailed histological examination in the attempt to
543 identify the processes underlying this phenomenon. The multilayered epithelium covering the
544 trabeculae (region 1) displayed increased cellularity with an increase in cell layers and

545 irregular arrangement, indicating hyperplasia (Fig. 2E). The epithelial hyperplasia extended to
546 the upper respiratory tract and was also observed in the trachea, larynx and nasal cavity. The
547 mid and basal areas of the faveolae (regions 2 and 3), where the epithelium is unilayered,
548 showed nuclear crowding which also suggested hyperplasia (Fig. 2E). The thickening
549 appeared to result from an increase in individual cell height, associated with a more columnar
550 appearance of the cells (Fig. 2E, F). Additionally, we noted an increase in septal connective
551 tissue (interstitial fibrosis). The described changes resulted in thickening of the septa and
552 narrowing of the faveolar lumen (Fig. 2D).
553 In the attempt to quantify the epithelial hyperplasia we measured the average total epithelial
554 height in the three defined regions (Figs. 2 and 9) in all diseased, i.e. RT-PCR-positive
555 animals in comparison to the RT-PCR-negative animals without pneumonia (controls). In all
556 locations, the epithelium was significantly (P <0.05 higher in the diseased animals than in the
557 control snakes (Fig. 10A; Table 4). Hyperplasia was confirmed in both lung (regions 1, 2 and
558 3) and trachea, where the average number of nuclei in the epithelial layer was significantly
559 higher in the diseased snakes (Fig 10B; Table 4).
560 Epithelial hyperplasia was associated with increased proliferative activity, as up to 90% of
561 epithelial cells in all lung regions and in the trachea were found to express PCNA in the
562 diseased animals (Fig. 11A). Alongside this, a moderate number of epithelial cells were found
563 to undergo apoptosis, based on cleaved caspase-3 staining (Fig. 11C). In comparison, control
564 animals exhibited rare PCNA-positive type II pneumocytes in all layers (Fig. 11B) as well as
565 scattered apoptotic (cleaved caspase-3 positive) type I and type II pneumocytes (Fig. 11D),
566 likely representing the physiological turnover of the epithelium.
567
568
569 **Discussion**

570 We initiated the present study by the urge to identify the causative agent for a fatal pneumonia
571 observed in green tree pythons (*Morelia viridis)*, characterised by the accumulation of mucoid
572 material in the airways and a histologically notable thickening of the lung epithelium. NGS
573 revealed the presence of a novel nidovirus, MVNV, which by phylogenetic analysis groups
574 with toroviruses. RT-PCR, immunohistology and RNA-ISH served to confirm its association
575 with the disease and to identify the viral target cells, i.e. epithelial cells in airways and the
576 luminal trabeculae, as well as the faveolar type I and II pneumocytes. We were able to isolate
577 and grow MVNV in both *M. viridis* and *B. constrictor* cell cultures. MVNV induced a
578 cytopathic effect both *in vitro* and *in vivo*. However, we also found nidovirus infection to
579 associate with generalised hyperplasia of the airway and lung epithelium which exhibited a
580 distinct proliferative activity and a degree of apoptotic cell death. Together these findings
581 would suggest nidovirus infection to increase the turnover of the epithelium. The mucus
582 accumulation in the air conducting space was accompanied by a significant increase in
583 secretory epithelial cells at the trabeculae and in (transformed) type II pneumocytes in the
584 faveolae, indicating increased mucus and/or surfactant production.
585 These results indicate that MVNV infects and damages the differentiated respiratory and
586 faveolar epithelium, but then persists and induces increased turnover of the infected epithelial
587 cells. The observed type II pneumocyte hyperplasia is obviously not specific to nidovirus
588 infection in the python, since it has been described in snakes as a consequence of pneumocyte
589 injury in a range of infectious diseases of viral, bacterial and mycotic nature (51, 58). It might
590 therefore represent an exaggerated regenerative attempt. Also in mammals type II
591 pneumocyte hyperplasia is seen as part of a lung defense mechanism to various insults (59–
592 61). In our cases, the hyperplastic epithelial cells exhibited abundant cytoplasmic
593 serous/mucous granules instead of the lamellar bodies that represent surfactant (50). This
594 suggests excess mucus and reduced surfactant production and release and would explain the
595 clinical findings (50, 58). Previous studies have shown that the surfactant of snakes, due to its

596 differing phospholipid composition, is likely less important for airway stabilisation, but rather
597 functions as an anti-adherent (also known as an "anti-glue") factor and an anti-oedemic factor
598 in the faveolar space (62); its reduction could therefore have added to the respiratory distress
599 observed in the affected snakes.
600 Increased turnover and/or hyperplasia of the epithelium has been described for several
601 coronaviridal diseases, such as infectious bronchitis in chickens, Breda virus infection in
602 calves, and coronavirus infection in rats (63–65). So far, however, the mechanisms underlying
603 this process have not been explained. Members of the subfamily *Torovirinae* are also known
604 to induce epithelial cell apoptosis (54, 66, 67); however, though our findings point towards
605 this, further studies are required to elucidate whether this also applies to MVNV and other
606 snake nidoviruses.
607 In our study, only fatal cases were examined. The pathological findings suggest that death
608 was mainly due to impaired gas exchange as a consequence of the type I pneumocyte loss. In
609 the healthy snake lung, thin cytoplasmic extensions of the type I pneumocytes cover the
610 capillary walls, forming the gas-blood barrier (50). Their replacement by mucus/surfactant-
611 secreting type II pneumocytes with their excessive height due to the cell crowding is unlikely
612 to allow effective gas exchange. With an average thickness of 24.40 µm (region 2) and 17.43
613 µm (region 3), the barrier was more than 1.7 x 10^4 times thicker than the normal blood-gas
614 barrier in the reptilian lung which ranges between 0.4 and 1 nm (50).
615 Further anatomical peculiarities of the *Morelia viridis* (or in general boid snake) lung could
616 have contributed to the fatal outcome of the disease (51, 68–70). Boidae have a well-
617 developed right lung and a rudimental left lung. The right lung displays two anatomically
618 distinct regions, the anterior region, which contains the profusely compartmented gas
619 exchange tissue, and the posterior saccular region, which is devoid of respiratory tissue and
620 has therefore been referred to as “air sac” (71, 72). The combination of elongated lungs and
621 caudal air sacs may contribute considerably to the outcome of the disease, as they create a

622 "cul-de-sac" that impairs removal of the mucus and thereby significantly reduces the air filled
623 space and the gas exchange capacity.
624 Though toroviruses mainly associate with enteric diseases, recent studies have shown that
625 they can be both entero- and pneumotropic (31, 73, 74). New nidoviruses were recently
626 identified in the lungs of cattle and wild shingleback lizards with pneumonia, though their
627 direct association with disease has so far not been examined (31, 56). We found MVNV-
628 associated lesions almost exclusively in the airways and lung, similar to previous reports on
629 nidovirus infections in other python species (8, 9, 15). The detection of viral RNA by PCR in
630 other tissues, such as liver, spleen, kidney and intestine, however, indicated that the viruses
631 spread systemically. We found further evidence of that, and of its pathogenicity, as we
632 detected nidovirus NP within a focal granulomatous-necrotising nephritis in one animal. We
633 also detected viral antigen in epithelial cells of the cranial oesophagus in one affected animal;
634 however, the oesophagus carries ciliated epithelium in *M. viridis* (data not shown), a feature
635 also known for other snake species (75, 76); infection could therefore be due to an overspill
636 from the trachea and nasal cavity. We did not detect viral antigen in any cells in stomach and
637 intestine, and neither did a previous study find viral RNA by ISH, suggesting that the python
638 nidoviruses are primarily respiratory (8). Spreading via the expelling of mucus from the nasal
639 cavity would be a likely route of transmission.
640
641
642 **Acknowledgements**
643 We are grateful to the technical staff of the Histology Laboratory and the Electron
644 Microscopy Unit, Institute of Veterinary Pathology, and to Elisabeth M. Schraner, Institute of
645 Virology and Institute of Veterinary Anatomy, Vetsuisse Faculty, University of Zurich, for
646 excellent technical support. We also thank our colleagues at the Institute of Veterinary

Bacteriology, Vetsuisse Faculty, University of Zurich, for performing the bacteriological examinations. Particular thanks are due to the breeders who submitted their snakes for diagnostic purposes.

References

1. McDiarmid RW, Campbell JA, Touré T. 1999. Snake Species of the World: A Taxonomic and Geographic Reference., Vol.1. Herpetologists' League, Washington, DC.
2. More G, Pantchev N, Herrmann DC, Vrhovec MG, Ofner S, Conraths FJ, Schares G. 2014. Molecular identification of Sarcocystis spp. helped to define the origin of green pythons (Morelia viridis) confiscated in Germany. Parasitology 141:646–651.
3. Nijman V, Shepherd CR. 2009. Wildlife trade from ASEAN to the EU: Issues with the trade in captive-bred reptiles from Indonesia. TRAFFIC Europe Report for the European Commission, Brussels, Belgium.
4. Rawlings LH, Donnellan SC. 2003. Phylogeographic analysis of the green python, Morelia viridis, reveals cryptic diversity. Molecular Phylogenetics and Evolution 27:36–44.
5. Aqrawi T, Stöhr AC, Knauf-Witzens T, Krengel A, Heckers KO, Marschang RE. 2015. Identification of snake arenaviruses in live boas and pythons in a zoo in Germany. Tierärztl Prax (K) 43:239–247.
6. Shaw G (ed.). 1802. General Zoology, Volume III, London.
7. Linné Cv, Salvius L. 1758. Systema naturae, Vol. 1. Holmiae:Impensis Direct. Laurentii Salvii.
8. Bodewes R, Lempp C, Schurch AC, Habierski A, Hahn K, Lamers M, Dornberg K von, Wohlsein P, Drexler JF, Haagmans BL, Smits SL, Baumgartner W, Osterhaus, A. D. M. E. 2014. Novel divergent nidovirus in a python with pneumonia. Journal of General Virology 95:2480–2485.
9. Stenglein MD, Jacobson ER, Wozniak EJ, Wellehan JFX, Kincaid A, Gordon M, Porter BF, Baumgartner W, Stahl S, Kelley K, Towner JS, DeRisi JL. 2014. Ball Python Nidovirus. A Candidate Etiologic Agent for Severe Respiratory Disease in Python regius. mBio 5:e01484-14-e01484-14.
10. Sun H, Lan D, Lu L, Chen M, Wang C, Hua X. 2014. Molecular characterization and phylogenetic analysis of the genome of porcine torovirus. Archives of virology 159:773–778.
11. Draker R, Roper RL, Petric M, Tellier R. 2006. The complete sequence of the bovine torovirus genome. Virus Research 115:56–68.
12. Fagerland JA, Pohlenz JFL, Woode GN. 1986. A Morphological Study of the Replication of Breda Virus (Proposed Family Toroviridae) in Bovine Intestinal Cells. Journal of General Virology 67:1293–1304.
13. Hoet AE, Cho K-O, Chang K-O, Loerch SC, Wittum TE, Saif LJ. 2002. Enteric and nasal shedding of bovine torovirus (Breda virus) in feedlot cattle. Am J Vet Res 63:342–348.
14. Woode GN, Reed DE, Runnels PL, Herrig MA, Hill HT. 1982. Studies with an unclassified virus isolated from diarrheic calves. Veterinary microbiology 7:221–240.
15. Uccellini L, Ossiboff RJ, Matos REC de, Morrisey JK, Petrosov A, Navarrete-Macias I, Jain K, Hicks AL, Buckles EL, Tokarz R, McAloose D, Lipkin W. 2014. Identification of a novel nidovirus in an outbreak of fatal respiratory disease in ball pythons (Python regius). Virol J 11:144.
16. Groot RJ de, Cowley JA, Enjuanes L, Faaberg KS, Perlman S, Rottier PJ, Snijder EJ, Ziebuhr J, Gorbalenya AE. 2011. Order nidovirales. Virus taxonomy:785–795.

17. Gorbalenya AE, Enjuanes L, Ziebuhr J, Snijder EJ. 2006. Nidovirales. Evolving the largest RNA virus genome. Virus Research 117:17–37.
18. Nga PT, del Carmen Parquet M, Lauber C, Parida M, Nabeshima T, Yu F, Thuy NT, Inoue S, Ito T, Okamoto K. 2011. Discovery of the first insect nidovirus, a missing evolutionary link in the emergence of the largest RNA virus genomes. PLoS Pathog 7:e1002215.
19. Lauber C, Ziebuhr J, Junglen S, Drosten C, Zirkel F, Nga PT, Morita K, Snijder EJ, Gorbalenya AE. 2012. Mesoniviridae: a proposed new family in the order Nidovirales formed by a single species of mosquito-borne viruses. Archives of virology 157:1623–1628.
20. Lauber C, Gorbalenya AE. 2012. Toward Genetics-Based Virus Taxonomy. Comparative Analysis of a Genetics-Based Classification and the Taxonomy of Picornaviruses. Journal of Virology 86:3905–3915.
21. Walker PJ, Winton JR. 2010. Emerging viral diseases of fish and shrimp. Veterinary Research 41:51.
22. Snijder EJ, Kikkert M, Fang Y. 2013. Arterivirus molecular biology and pathogenesis. J Gen Virol 94:2141–2163.
23. To KKW, Hung IFN, Chan JFW, Yuen K-Y. 2013. From SARS coronavirus to novel animal and human coronaviruses. Journal of Thoracic Disease 5 Suppl 2:8.
24. Baird A, Faisal M. 2016. Fathead minnow nidovirus infects spotfin shiner Cyprinella spiloptera and golden shiner Notemigonus crysoleucas. Dis. Aquat. Org. 119:37–44.
25. McVey DS, Kennedy M, Chengappa MM (ed.). 2013. Veterinary Microbiology, 3. Aufl. Wiley-Blackwell, New Jersey.
26. Beards GM, Campbell AD, Cottrell NR, Peiris JS, Rees N, Sanders RC, Shirley JA, Wood HC, Flewett TH. 1984. Enzyme-linked immunosorbent assays based on polyclonal and monoclonal antibodies for rotavirus detection. Journal of clinical microbiology 19:248–254.
27. Weiss M, Steck F, Horzinek MC. 1983. Purification and partial characterization of a new enveloped RNA virus (Berne virus). Journal of General Virology 64:1849–1858.
28. Cann AJ. 2001. Chapter 2-Particles. The function and formation of virus particles, p. 25–27. *In* Cann AJ (ed), Principles of Molecular Virology (Standard Edition). Elsevier, Academic Press, London.
29. Cornelissen LA, van Woensel PA, Groot RJ de, Horzinek MC, Visser N, Egberink HF. 1998. Cell culture-grown putative bovine respiratory torovirus identified as a coronavirus. Vet Rec 142:683–686.
30. Vanopdenbosch E, Wellemans G, Petroff K. 1991. Breda virus associated with respiratory disease in calves. Vet Rec 129:203.
31. Tokarz R, Sameroff S, Hesse RA, Hause BM, Desai A, Jain K, Lipkin WI. 2015. Discovery of a novel nidovirus in cattle with respiratory disease. J Gen Virol 96:2188–2193.
32. Smits SL, Lavazza A, Matiz K, Horzinek MC, Koopmans MP, de Groot RJ. 2003. Phylogenetic and evolutionary relationships among torovirus field variants: evidence for multiple intertypic recombination events. Journal of Virology 77:9567–9577.
33. Petric M. 2003. Section VI. Other viruses causing gastroenteritis. Epidemiology of toroviruses. *In* Desselberger U, Gray J (ed), Viral Gastroenteritis, 9th ed. Elsevier, Amsterdam.
34. Snijder EJ, Ederveen J, Spaan WJ, Weiss M, Horzinek MC. 1988. Characterization of Berne virus genomic and messenger RNAs. J Gen Virol 69:2135–2144.
35. Hetzel U, Sironen T, Laurinmaki P, Liljeroos L, Patjas A, Henttonen H, Vaheri A, Artelt A, Kipar A, Butcher SJ, Vapalahti O, Hepojoki J. 2013. Isolation, identification, and characterization of novel arenaviruses, the etiological agents of boid inclusion body disease. Journal of Virology 87:10918–10935.
36. Li H, Durbin R. 2010. Fast and accurate long-read alignment with Burrows-Wheeler transform. Bioinformatics 26:589–595.

37. Okonechnikov K, Golosova O, Fursov M. 2012. Unipro UGENE: a unified bioinformatics toolkit. Bioinformatics 28:1166–1167.
38. Tamura K, Stecher G, Peterson D, Filipski A, Kumar S. 2013. MEGA6. Molecular Evolutionary Genetics Analysis Version 6.0. Molecular Biology and Evolution 30:2725–2729.
39. Drummond AJ, Suchard MA, Xie D, Rambaut A. 2012. Bayesian phylogenetics with BEAUti and the BEAST 1.7. Molecular Biology and Evolution 29:1969–1973.
40. Rambaut A., Suchard MA., Xie D., Drummond AJ. 2014. Tracer v1.6. Beast Bio. http://beast.bio.ed.ac.uk/Tracer.
41. Zuker M. 2003. Mfold web server for nucleic acid folding and hybridization prediction. Nucleic Acids Res 31:3406–3415.
42. Edgar RC. 2004. MUSCLE: multiple sequence alignment with high accuracy and high throughput. Nucleic Acids Res 32:1792–1797.
43. Finn RD, Clements J, Eddy SR. 2011. HMMER web server. Interactive sequence similarity searching. Nucleic Acids Res 39:W29-W37.
44. Hepojoki J, Kipar A, Korzyukov Y, Bell-Sakyi L, Vapalahti O, Hetzel U. 2015. Replication of boid inclusion body disease-associated arenaviruses is temperature sensitive in both boid and mammalian cells. J. Virol. 89:1119–1128.
45. Korzyukov Y, Hetzel U, Kipar A, Vapalahti O, Hepojoki J. 2016. Generation of Anti-Boa Immunoglobulin Antibodies for Serodiagnostic Applications, and Their Use to Detect Anti-Reptarenavirus Antibodies in Boa Constrictor. PLoS One 11:e0158417.
46. Ressel L, Ward S, Kipar A. 2015. Equine Cutaneous Mast Cell Tumours Exhibit Variable Differentiation, Proliferation Activity and KIT Expression. J Comp Pathol 153:236–243.
47. Antoine DJ, Williams DP, Kipar A, Laverty H, Park BK. 2010. Diet Restriction Inhibits Apoptosis and HMGB1 Oxidation and Promotes Inflammatory Cell Recruitment during Acetaminophen Hepatotoxicity. Molecular Medicine 16:479–490.
48. Swadzba E, Rupik W. 2010. Ultrastructural studies of epidermis keratinization in grass snake embryos Natrix natrix L. (Lepidosauria, Serpentes) during late embryogenesis. Zoology (Jena) 113:339–360.
49. Wang F, Flanagan J, Su N, Wang L-C, Bui S, Nielson A, Wu X, Vo H-T, Ma X-J, Luo Y. 2012. RNAscope: a novel in situ RNA analysis platform for formalin-fixed, paraffin-embedded tissues. J Mol Diagn 14:22–29.
50. Pastor LM. 1995. Chapter 5- The histology of the reptilian lung, p. 127–155. *In* Pastor LM (ed), Histology, ultrastructure and immunohistochemistry of the respiratory organs in non mammalian vertebrates, 1st ed. Secretariado de Publicaciones de la Univesidad de Murcia, Murcia.
51. Starck JM, Weimer I, Aupperle H, Muller K, Marschang RE, Kiefer I, Pees M. 2015. Morphological Pulmonary Diffusion Capacity for Oxygen of Burmese Pythons (Python molurus): a Comparison of Animals in Healthy Condition and with Different Pulmonary Infections. J Comp Pathol 153:333–351.
52. Maina JN. 1989. The morphology of the lung of the black mamba Dendroaspis polylepis (Reptilia: Ophidia: Elapidae). A scanning and transmission electron microscopic study. Journal of Anatomy 167:31–46.
53. Perry SF. 1983. 1. Introduction. Descriptive Classification of Lung Types. Histological Structure, p. 1–3. *In* Perry SF (ed), Reptilian lungs: functional anatomy and evolution. Springer Verlag, Berlin.
54. Kuwabara M, Wada K, Maeda Y, Miyazaki A, Tsunemitsu H. 2007. First Isolation of Cytopathogenic Bovine Torovirus in Cell Culture from a Calf with Diarrhea. Clinical and Vaccine Immunology 14:998–1004.

55. Huder JB, Boni J, Hatt J-M, Soldati G, Lutz H, Schupbach J. 2002. Identification and characterization of two closely related unclassifiable endogenous retroviruses in pythons (Python molurus and Python curtus). J. Virol. 76:7607–7615.
56. O'Dea MA, Jackson B, Jackson C, Xavier P, Warren K. 2016. Discovery and Partial Genomic Characterisation of a Novel Nidovirus Associated with Respiratory Disease in Wild Shingleback Lizards (Tiliqua rugosa). PLoS One 11:e0165209.
57. Shi W, Zhang Z, Ling C, Carr MJ, Tong Y, Gao GF. 2016. Increasing genetic diversity of Zika virus in the Latin American outbreak. Emerg Microbes Infect 5:e68. doi:10.1038/emi.2016.68.
58. Jacobson ER, Adams HP, Geisbert TW, Tucker SJ, Hall BJ, Homer BL. 1997. Pulmonary Lesions in Experimental Ophidian Paramyxovirus Pneumonia of Aruba Island Rattlesnakes, Crotalus unicolor. Veterinary Pathology 34:450–459.
59. Ward HE, Nicholas TE. 1984. Alveolar type I and type II cells. Aust N Z J Med 14:731–734.
60. Fehrenbach H, Kasper M, Tschernig T, Pan T, Schuh D, Shannon JM, Muller M, Mason RJ. 1999. Keratinocyte growth factor-induced hyperplasia of rat alveolar type II cells in vivo is resolved by differentiation into type I cells and by apoptosis. European Respiratory Journal 14:534–544.
61. Caswell JL, Williams KJ. 2016. Chapter 5 - Respiratory System, 465-591. *In* Maxie MG (ed), Jubb, Kennedy & Palmer's Pathology of Domestic Animals, 6th ed., vol. 2. Elsevier, St. Louis, Missouri.
62. Veldhuizen R, Nag K, Orgeig S, Possmayer F. 1998. The role of lipids in pulmonary surfactant. Biochimica et Biophysica Acta (BBA) - Molecular Basis of Disease 1408:90–108.
63. Grgiæ H, Hunter DB, Hunton P, Nagy É. 2008. Pathogenicity of infectious bronchitis virus isolates from Ontario chickens. Canadian Journal of Veterinary Research 72:403–410.
64. Schunk MK, Percy DH, Rosendal S. 1995. Effect of time of exposure to rat coronavirus and Mycoplasma pulmonis on respiratory tract lesions in the Wistar rat. Canadian Journal of Veterinary Research 59:60–66.
65. Koopmans M, Horzinek MC. 1995. The Pathogenesis of Torovirus Infections in Animals and Humans, p. 403–413. *In* Siddell SG (ed), The Coronaviridae. Springer US, Boston, MA.
66. Maestre AM, Garzon A, Rodriguez D. 2011. Equine torovirus (BEV) induces caspase-mediated apoptosis in infected cells. PLoS One 6:e20972.
67. Ding X, Xu F, Chen H, Tesh RB, Xiao S-Y. 2005. Apoptosis of Hepatocytes Caused by Punta Toro Virus (Bunyaviridae. Phlebovirus) and Its Implication for Phlebovirus Pathogenesis. The American Journal of Pathology 167:1043–1049.
68. Stinner JN. 1987. Gas exchange and air flow in the lung of the snake, Pituophis melanoleucus. Journal of Comparative Physiology B 157:307–314.
69. van Wallach. 1998. The lungs of snakes. Biology of the Reptilia 19:93–295.
70. Perry SF, Bauer AM, Russell AP, Alston JT, Maloney JE. 1989. Lungs of the gecko Rhacodactylus leachianus (reptilia: Gekkonidae): A correlative gross anatomical and light and electron microscopic study. J. Morphol. 199:23–40.
71. McDonald HS. 1959. Respiratory functions of the ophidian air sac. Herpetologica 15:193–198.
72. Stinner HN. 1982. Ventillation, gas exchange and blood gases in the snake, Pituophis melanoleucus. Respiration physiology 47:279–298.
73. Saif LJ, Bohl EH. 1986. Transmissible gastroenteritis, 255-274. *In* Leman AD, Straw B, Glock RD (ed.), Diseases of swine, 6th ed. Iowa State University Press, Iowa.
74. Koopmans M, Horzinek MC. 1994. Toroviruses of animals and humans. A review. Adv Virus Res 43:233–273.
75. Imai M, Shibata T, Moriguchi K. 1991. Pepsinogen granules in the esophageal epithelium of the rock snake. Okajimas Folia Anat Jpn 68:231–234.
76. Cundall D, Tuttman C, Close M. 2014. A model of the anterior esophagus in snakes, with functional and developmental implications. Anat Rec (Hoboken) 297:586–598.

Figure Legends

Figure 1: Gross findings in a green tree python (*Morelia viridis*) with nidovirus-associated proliferative pneumonia (animal E1). Both trachea (A) and lungs (B) are filled with abundant mucoid material (arrows). H - heart.

Figure 2: Histological findings in *Morelia viridis* with nidovirus-associated proliferative pneumonia. **A-C**. Uninfected control case (animal G2). Representative photomicrographs of a healthy lung (cross section). Thin pulmonary septa form the faveolar spaces. At the luminal end, the septa exhibit bundles of smooth muscle cells (myoelastic bundles) that form contractile trabeculae. For detailed assessments, three regions (1, 2, 3) were identified. The trabeculae are covered by a multilayered pseudostratified "bronchial-type" epithelium, dominated by ciliated cells (B1, C1). In regions 2 (B2, C2) and 3 (B3, C3), the faveolae are covered by a single-layered "gas exchange epithelium" comprised of flat type I pneumocytes (arrowheads); surfactant producing type II pneumocytes (arrows) are less abundant. **D-F**. Snake with nidovirus infection (animal B4). Representative photomicrograph of a diseased lung (cross section). In the entire lung, the epithelial layer is thickened due to hyperplasia. The faveolar space (3) is filled with proteinaceous material and the interstitium is broadened due to a mixed inflammatory infiltrate (E1, 2). In region 1 (E1, F1), the pseudostratified epithelium covering the trabeculae exhibits increased cellularity with an increase in cell layers and irregular arrangement (hyperplasia) as well as a loss of cilia and several apoptotic epithelia cells (arrowheads). In regions 2 (E2, F2) and 3 (E3, F3), type I pneumcytes are almost entirely replaced by large, columnar type II pneumocytes. A, B, D, E: HE stain; C, F: IH for cytokeratin, haematoxylin counterstain. Bars = 100 µm (A, D) and 10 µm (B, C, E, F).

Figure 3: Virus isolation in a primary *Morelia viridis* foetal brain cell culture. **A**. Uninfected control cells. **B, C**. Cells after inoculation with lung homogenate from a diseased snake (animal C2). First evidence of a cytopathic effect is seen after 2 days (B), as enlargement,

rounding, and cytoplasmic vacuolisation as well as loss of adherence (arrows). After 6 days (C), only few intact cells have remained. Most cells are detached and necrotic. **D, E**. Ultramicrographs of a cell pellet prepared at 1 dpi. There are abundant tubular structures arranged in stacks within the cytoplasm of infected cells. **F**. Concentrated supernatant of the infected cells, negative staining. Rod- and kidney-shaped virions of approximately 120 nm length. Bar = 1 µm (D) and 100 nm (E).

Figure 4. Morelia viridis nidovirus, MVNV, genome organization, NGS coverage, and phylogenetic relationship to related viruses. **A**. A schematic representation of the untranslated regions (UTRs) and open reading frames (ORFs) of the 32,414 nt ssRNA+ genome of MVNV. **B.** Alignment around the ribosomal frameshift signal (RFS, indicated by an arrow in the alignment and structure prediction) in nidoviruses identified in pythons with ORF1a stop codon highlighted. A prediction for the RNA structure around the RFS in MVNV, the arrow highlights a difference to the structure described by Bodewes et al. (8) **C**. The contig coverage, y-axis shows the number of reads matching each nucleotide position (x-axis) of the contig. Bowtie2 was used to map the reads to the contig generated by de novo assembly. **D.** Virus growth in different cell lines. Cell culture supernatant of the indicated cell lines inoculated with MVNV was analyzed by qRT-PCR at the indicated time points. The fold increase indicates viral RNA increase in the cell culture supernatant as compared to the amount detected at 0 dpi.

Figure 5. Immunofluorescence staining of *M. viridis* and *B. constrictor* cell lines with anti-MVNV NP antiserum at 1:2,000 dilution. MVNV- or mock-infected cells were stained at 3 dpi, and recorded at 40x under inverted fluorescence microscope. Mock infected cells are shown on the right and MVNV infected cells on the left. DAPI is shown in blue and MVNV specific staining in red.

885 **Figure 6**. Maximum clade credibility tree constructed from ORF1b amino acid sequences of
886 the representatives of the subfamily Torovirinae. The phylogenetic tree was constructed using
887 Bayesian MCMC method with LG+G+I model of substitution. Posterior probabilities are
888 shown in each node.

889 **Figure 7.** Changes in the lung epithelium in *Morelia viridis* with nidovirus-associated
890 proliferative pneumonia. Representative photomicrographs (A, C, E, animal B4) and
891 ultramicrographs (B, D, F, animal A1) of diseased lungs (cross sections). **A, B**. Region 1. **A**.
892 The PAS/Alcian Blue stain highlights positive (arrowheads) secretory epithelial cells in all
893 cell layers of the hyperplastic multilayered trabecular epithelium. Abundant mucus fills the
894 lumen. **B**. The ultrastructural features of most cells (cytoplasmic mucous granules and short
895 microvilli) show that they are secretory cells (50). Only a few ciliated cells are seen (arrow).
896 **C-F**. In regions 2 (C, D) and 3 (E, F), the faveolae are diffusely lined by cuboidal cells
897 containing serous/mucous granules (C, E, arrowheads), consistent with type II pneumocytes.
898 Ultrastructurally, these cells resemble so-called "transformed" type II pneumocytes, as they
899 contain serous/mucous granules (arrows) and lack the lamellar bodies characteristic for
900 normal type II pneumocytes (51).

901 **Figure 8.** Viral target cells in lungs and airways of *Morelia viridis* with nidovirus-associated
902 proliferative pneumonia. **A-D**. Animals A1 (A) and A2 (B-D), lung. The pseudostratified
903 trabelular epithelium (region 1) exhibits abundant viral RNA mainly in superficial epithelial
904 cell layers (**A**). **B**. Viral antigen expression is seen in all cell layers. In basal and mid layers, it
905 is represented by a focal cytoplasmic reaction (arrowhead). The fully differentiated superficial
906 epithelial cells exhibit abundant viral antigen (arrow) and loss of cilia. Infected cells are also
907 found shed into the lumen. **C**. Region 2. In areas with intact faveolar epithelium, both type I
908 (arrowhead) and differentiated type II pneumocytes (arrows) exhibit strong viral antigen
909 expression. The new, hyperplastic type II pneumocytes in other areas display a weaker focal

cytoplasmic reaction (arrows). At the base of the faveolae (**D**), type I (arrowheads) and type II (arrows) pneumocytes are also found to be infected. They are also shed into the faveolar lumen. **E**. Animal A1, nasal cavity. The epithelium is thickened due to hyperplasia and exhibits nidovirus infection mainly of the fully differentiated superficial epithelial cells (arrow). C - cartilage. **F**. Animal A1, trachea. Bottom: The ciliated epithelium is largely intact (arrow), but there are scattered individual or small groups of infected cells. Sloughed, degenerate epithelial cells are also found to carry viral RNA (arrowhead). Top: Infected cells are intact (arrowhead) or degenerate, shedding virus (arrow). C – tracheal ring cartilage. RNA-ISH (RNAscope technology; A, E, F) and IH (HRP method; B-D) for MVNV N protein, haematoxylin counterstain. Bars = 20 µm (A, E, F bottom) and 10 µm (B-D, F top). **G**. Ultramicrograph of a type II pneumocyte with staples of tubular structures of 100 – 150 nm length (arrows). Bar = 1 µm.

Figure 9. Illustration of the morphometric approach taken to measure the epithelial height and number of epithelial cell nuclei in cytokeratin-stained cross sections of the lungs. **A**. Three regions were defined in the proximal, bronchiolar lung: 1) The luminal part of the primary trabeculae, covered by a multilayered pseudostratified ciliated epithelium (1). 2) The faveolae at mid level (2) and at the base (3), covered by a single layered epithelium. **B.** Region 1, measurement of epithelial height. The blue lines represent 10 measurements taken over a 300 µm wide epithelial segment, determining the distance between the apical epithelial cell border and the basal membrane. 200-fold magnification. **C.** Region 1, determination of cell number. The total amount of epithelial nuclei (x) counted in a 200 µm wide epithelial segment. 400-fold magnification. **D, E.** Region 2 (D) and 3 (E), measurement of epithelial height. The blue lines represent 10 measurements taken over a 300 µm wide epithelial segment, determining the distance between the apical epithelial cell border and the basal membrane. 200-fold magnification.

935 **Figure 10**.The average epithelial height measured in three lung regions and the trachea of
936 infected animals (white) was significantly higher than in non-infected (control) animals
937 (gray). Box plots illustrate the third quartile (Q3) and first quartile (Q1) range of the data,
938 filled circles represent data outliers (>1.5x interquartile range). Boxplots were created by
939 the SPSS Statistics software. A Mann-Whitney U test for independent samples (t-test) was
940 used for statistical analysis, and a p-value of less than 0.05 was considered significant
941 **Figure 11.** Increased epithelial turnover in the lungs of *Morelia viridis* with nidovirus-
942 associated proliferative pneumonia. Trabeculae (region 1). **A, C**. Diseased animal (C1). The
943 hyperplastic pseudostratified epithelium is proliferating, as confirmed by the PCNA
944 expression in almost all epithelial cells. Infiltrating lymphocytes (arrow; **A**) are also positive.
945 There are also abundant, cleaved caspase 3-positive apoptotic epithelial cells (**C**). A
946 proportion of infiltrating leukocytes is also found to undergo apoptosis (arrow; C). **B, D**.
947 Control animal (G3). In the control animal, only scattered individual basal epithelial cells are
948 found to express PCNA (arrowhead; **B**). Similarly, only rare epithelial cells are found to
949 undergo apoptosis (arrowhead; **D**). Apoptosis (i.e. cleaved caspase-3 expression) is also seen
950 in occasional lymphocytes (arrow) of the lymphoid aggregates. IH for PCNA (A, B) and
951 cleaved caspase-3 (C, D), HRP method, haematoxylin counterstain. Bars = 20 µm.

Table 1. Animals

A. Animals tested positive for MVNV by RT-PCR, RNA-ISH and IH

Animal	Age (y)	Sex	Clinical signs	Diagnostic tests*
A1	1	M	No history	Bacteriology
A2	5	F	Sudden death	NGS
A3	8	M	Sudden death, mucus in oral cavity	Bacteriology
A4	np	F	Acute respiratory distress (1 day)	
B1	6	M	Respiratory distress (3-4 days), expulsion of mucus	Virology, virus isolation, NGS
B2	7	F	Respiratory distress (3-4 days), expulsion of mucus	Virology
C1	2.5	M	Chronic anorexia, acute respiratory distress	Virology
C2	8	M	Respiratory distress	Virus isolation
D1	6	F	Respiratory distress (≥ 1 week)	NGS
E1	np	F	Respiratory distress (≥ 1 week)	
F1	2	F	Sudden death	
G1	6	F	Sudden death	

A - G: Breeding collections; Bacteriology – routine bacteriological examination performed on lungs; Virology – lung tissue screened for viruses (reovirus, paramyxovirus, Sunshine virus, nidovirus) in a commercial laboratory; NGS – Next generation sequencing on lung homogenates; y – years; np – not provided (adult); M – male, F – female; *Tests performed prior to or alongside MVNV RT-PCR, IHC and RNA-ISH

B. Uninfected control animals (negative for MVNV by RT-PCR)

Animal	Age (y)	Sex	Clinical signs	Diagnosis
G2	9	M	Sudden death	Mild colitis
G3	6	F	Emaciation, death	Mild enteritis and nephritis
G4	2	F	Sudden death	BIBD, severe purulent vasculitis around oesophagus and trachea
G5	1	M	Sudden death	Focal suppurative pneumonia in one lobe

G: Breeding collection; y – years; M – male, F – female;

Table 2. HMMER3 analysis of functional domains in the ORFs detected in MVNV genome.

			Alignment			E-value		
	Family id	Accession	Start	End	Bit Score	Independe	Condition	Description
ORF1a	Methyltransf_25	PF13649.5	3075	3150	15.08	0.027	4.80E-06	Methyltransferase domain
	zf-CCCH	PF00642.23	1052	1072	12.09	0.13	2.40E-05	Zinc finger C-x8-C-x5-C-x3-H type
		PF00642.23	1098	1117	9.91	0.64	0.00011	Zinc finger C-x8-C-x5-C-x3-H type
ORF1b	NSP13	PF06460.11	2077	2239	50.2	1.80E-13	1.20E-16	Coronavirus NSP13
	Viral_helicase1	PF01443.17	1144	1380	45.91	5.20E-12	3.40E-15	Viral (Superfamily 1) RNA helicase
	AAA_30	PF13604.5	1101	1231	42.93	3.90E-11	2.60E-14	AAA domain
	RdRP_1	PF00680.19	479	651	40.69	1.00E-10	6.60E-14	RNA dependent RNA polymerase
	AAA_19	PF13245.5	1100	1229	33.98	3.10E-08	2.00E-11	AAA domain
ORF5	Arteri_nucleo	PF01481.15	32	132	23.35	5.50E-05	9.90E-09	Arterivirus nucleocapsid protein

Table 3. Nucleotide and amino acid identities comparing MVNV and the nidoviruses identified in *Python molurus* (Indian python) and *Python regius* (ball python).

	Nucleotide		Amino acid	
	Python nidovirus S1536/13 (KJ935003)	Ball python nidovirus 07-53 (KJ541759)	Python nidovirus S1536/13 (KJ935003)	Ball python nidovirus 07-53 (KJ541759)
5´ UTR	85.1	87.0		
ORF1a	72.8	72.8	69.5	69.6
ORF1b	86.5	86.3	91.0	90.5
ORF2	80.9	80.0	85.0	84.8
ORF3	69.5	67.0	64.7	65.4
ORF4	76.5	79.2	83.3	82.9
ORF5	75.1	74.0	74.2	74.8
ORF6	65.6	66.9	59.7	59.2
ORF7	77.1	78.6	68.8	71.9
3´ UTR	95.2	93.9		
Complete genome/CDS	77.3	77.3	77.2	77.1

In brackets: Genebank accession numbers.

Table 4. Results of the quantitative assessment of epithelial height and cellularity in lung and trachea of MVNV-positive animals (tested positive by RT-PCR, RNA-ISH and IH; n=12) in comparison to uninfected control animals (negative for MVNV by RT-PCR and IH; n=4).

A. Lungs

	MVNV-positive animals[1]		Uninfected control animals[2]	
	Epithelial height (µm)[1]	Number of nuclei[1]	Epithelial height (µm)[1]	Number of nuclei[1]
Region 1	62.97±25.39	62.97±25.39	24.96±26.13	6.54±0.81
Region 2	24.4±14.16	14.97±3.57	6.61±14.59	8.83±0.76
Region 3	17.43±8.1	15.22±2.66	6.46±8.41	10.33±0.85

For all regions, the values are significantly different between infected and control animals ($P < 0.05$).
1 Mean ± standard deviation

B. Trachea

MVNV-positive animals[1]		Uninfected control animals[2]	
Epithelial height (µm)[1]	Number of nuclei[1]	Epithelial height (µm)[1]	Number of nuclei[1]
61.5±14.06	82.33±39.15	28.21±5.74	44.25±12.09

Values are significantly different between infected and control animals ($P < 0.05$).
1 Mean ± standard deviation

Lung regions 1-3: 1) Multilayered pseudostratified epithelium covering the luminal part of the primary trabeculae; 2) Single layered epithelium at mid level of the faveolae; and 3) Single layered epithelium at the base of the faveolae.

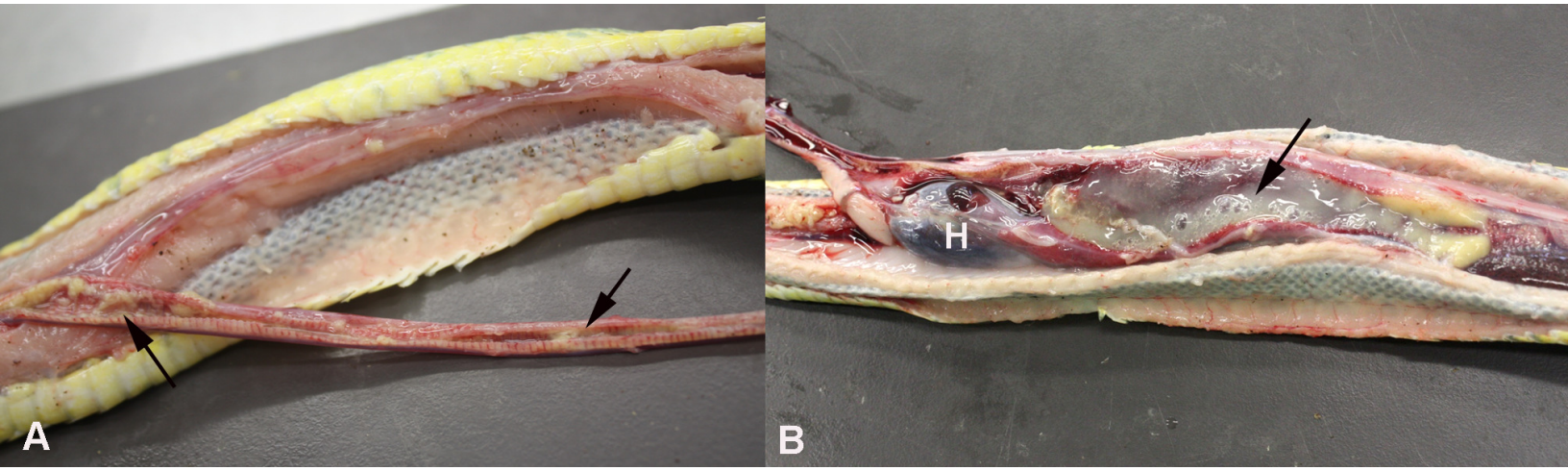
A
H
B

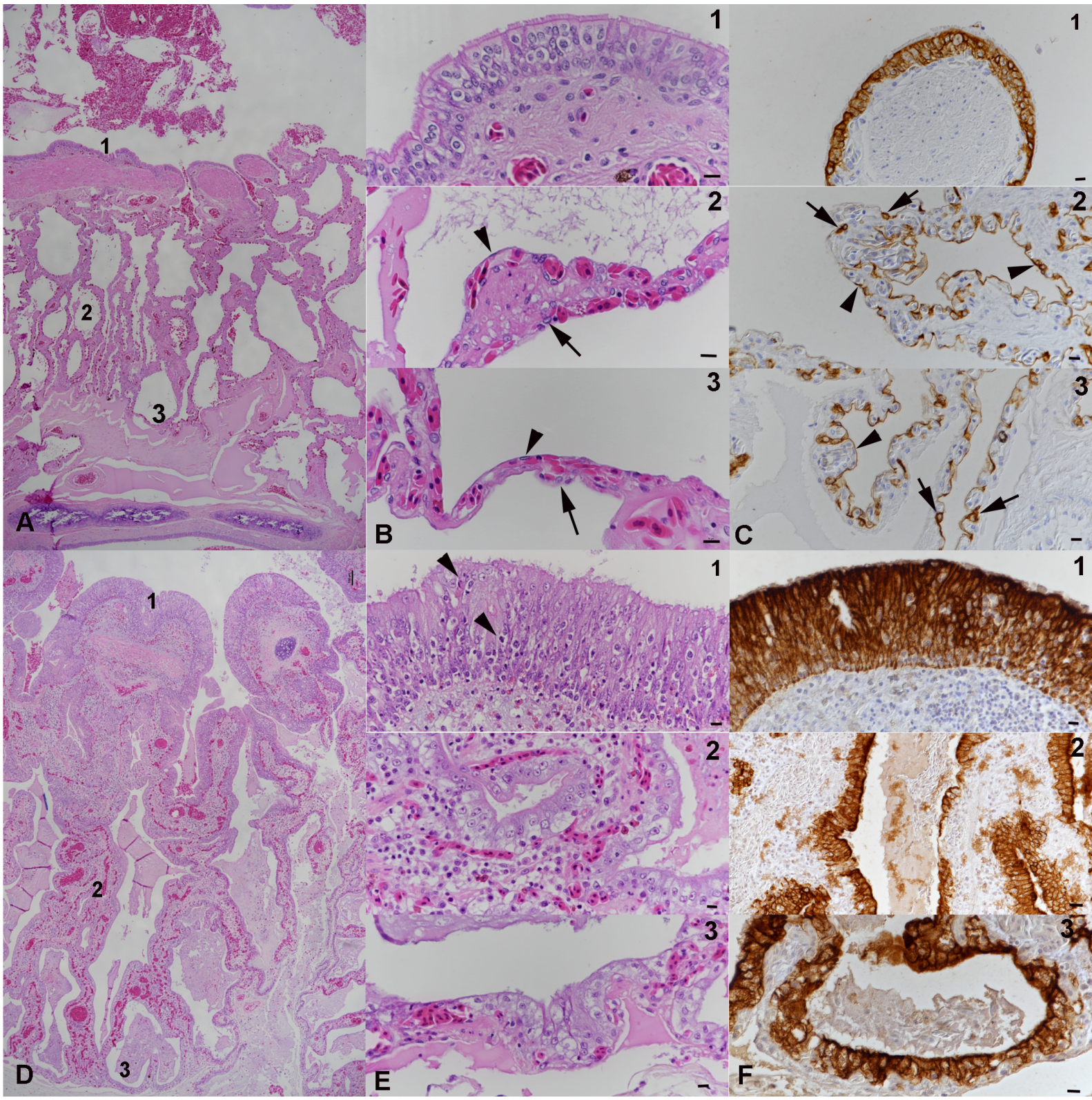
Uninfected control case
Snake with nidovirus infection
A
B
C
D
E
F
1
2
3

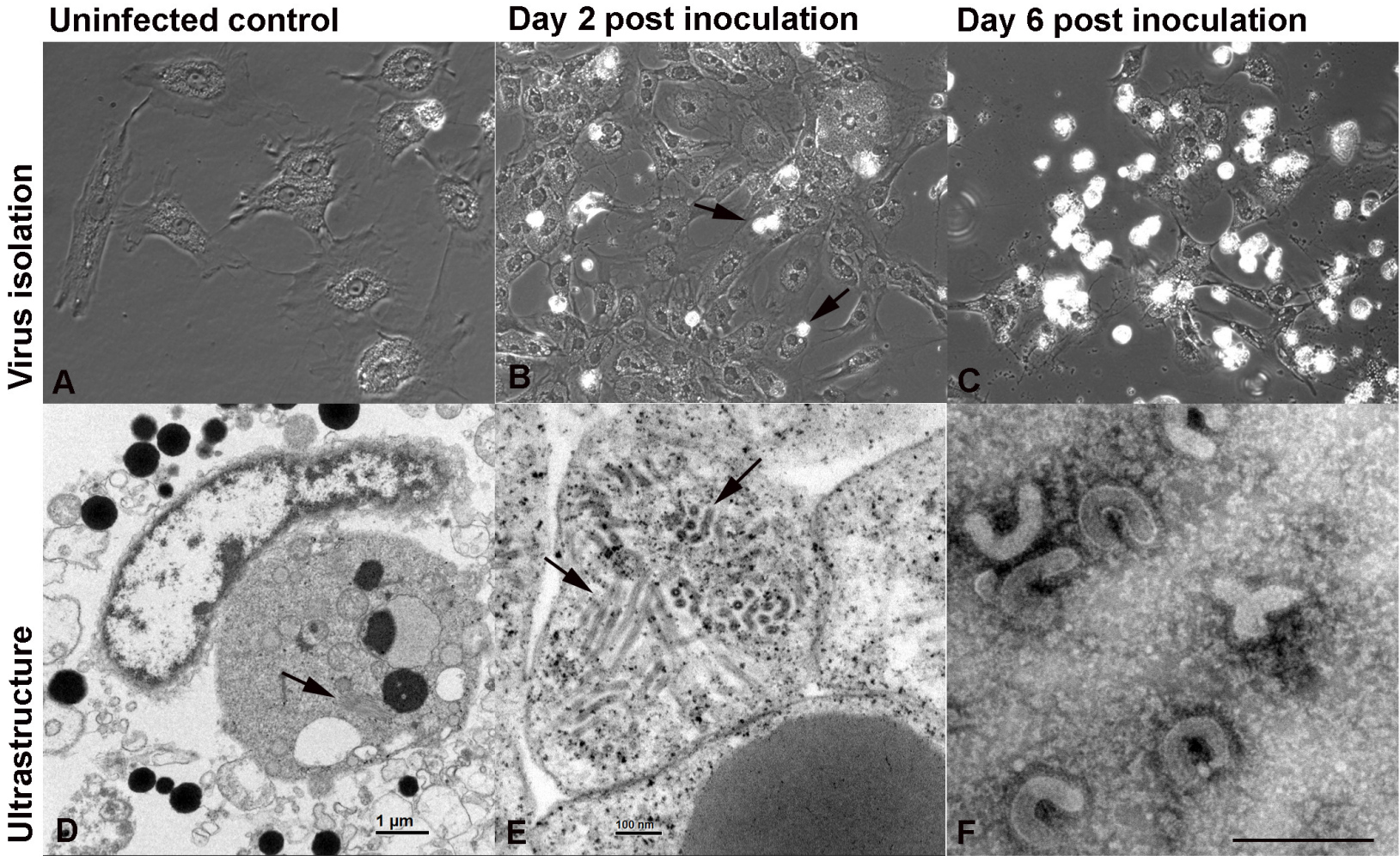
Uninfected control
Day 2 post inoculation
Day 6 post inoculation
Virus isolation
Ultrastructure
A
B
C
D
E
F
1 µm
100 nm

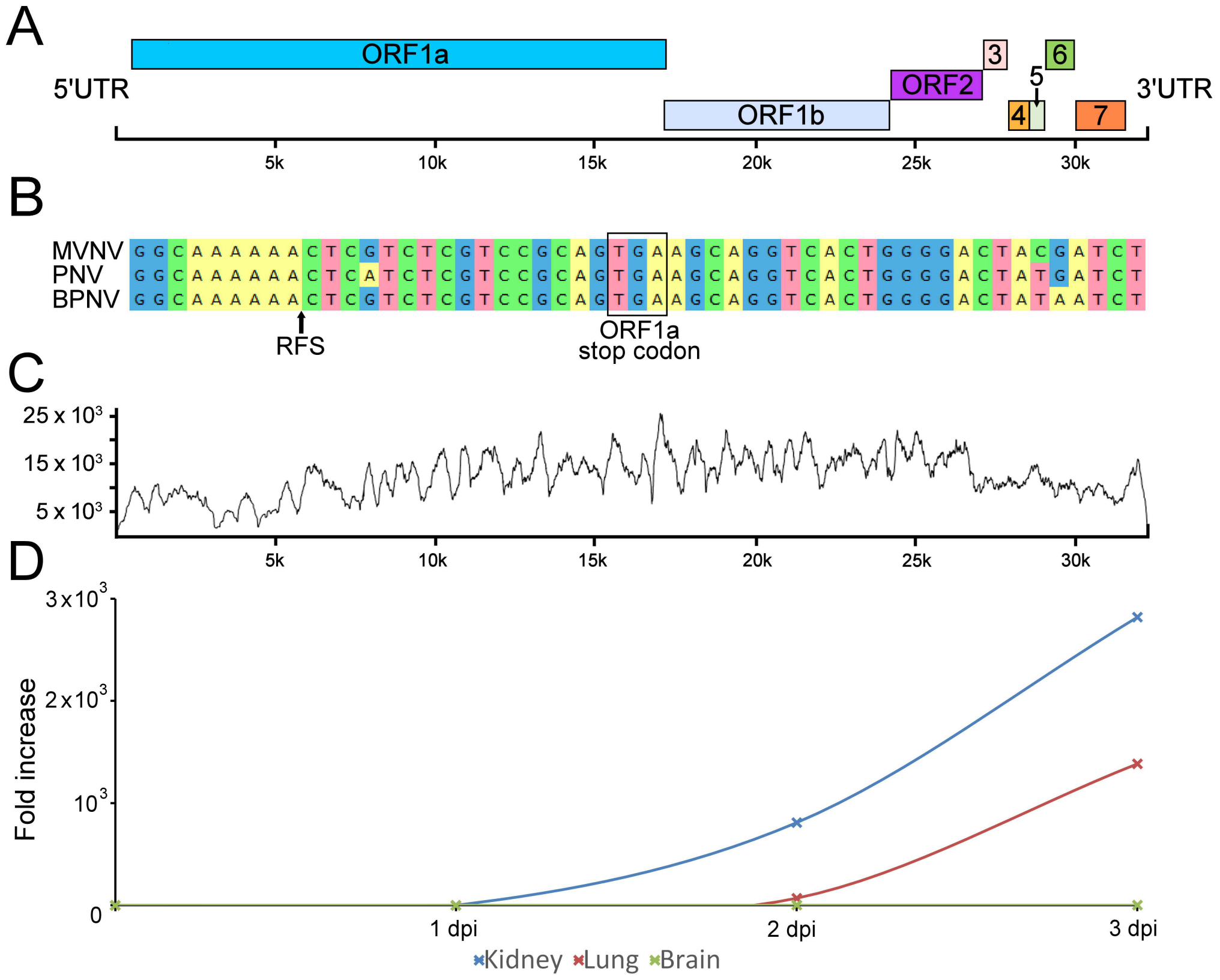
A
ORF1a
5'UTR
3'UTR
ORF2
ORF1b
3
6
5
4
7
5k
10k
15k
20k
25k
30k
B
MVNV
PNV
BPNV
RFS
ORF1a
stop codon
C
25 x 10³
15 x 10³
5 x 10³
5k
10k
15k
20k
25k
30k
D
3x10³
2x10³
10³
0
Fold increase
1 dpi
2 dpi
3 dpi
Kidney
Lung
Brain

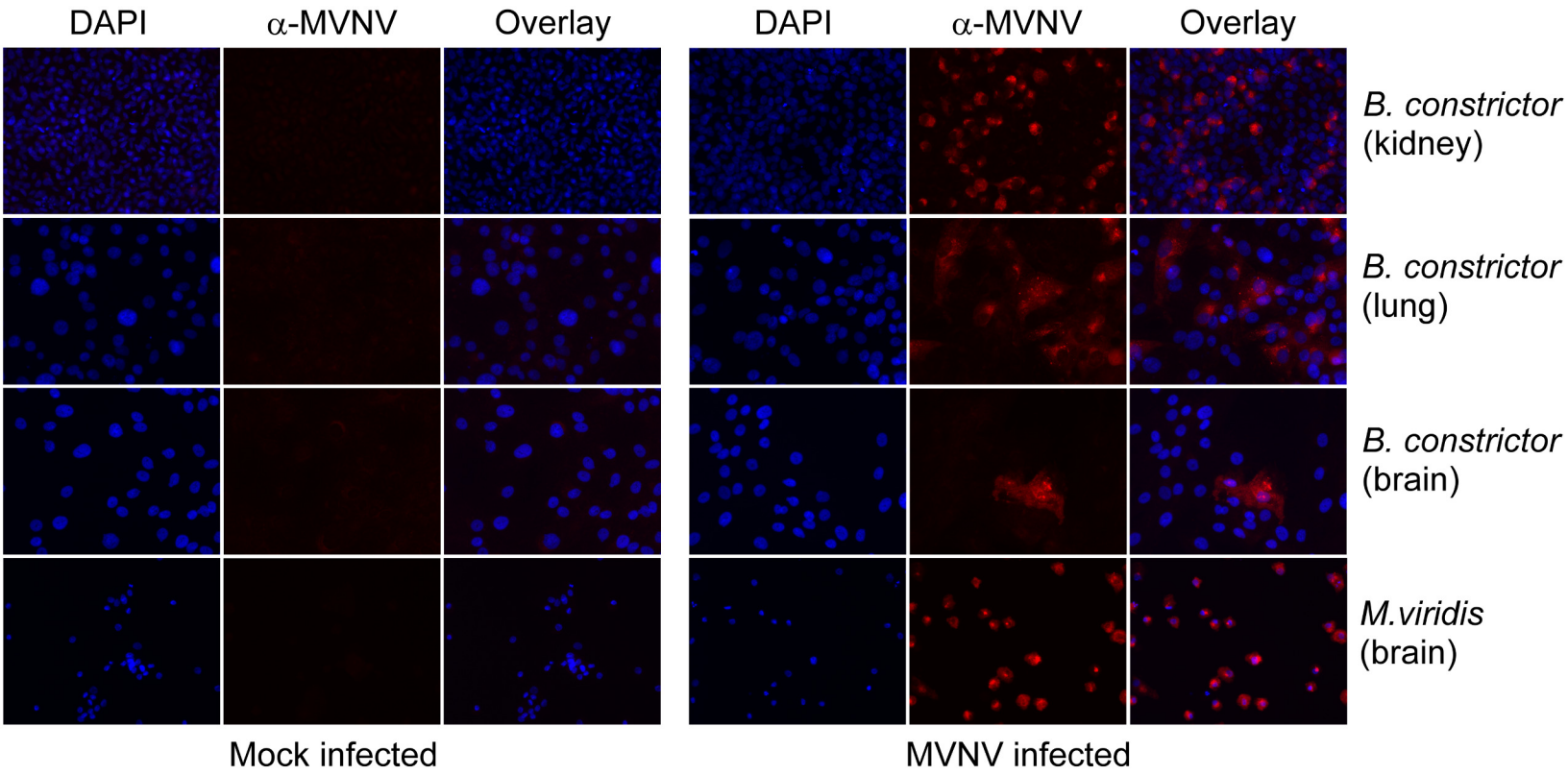
DAPI
α-MVNV
Overlay
DAPI
α-MVNV
Overlay
B. constrictor (kidney)
B. constrictor (lung)
B. constrictor (brain)
M.viridis (brain)
Mock infected
MVNV infected

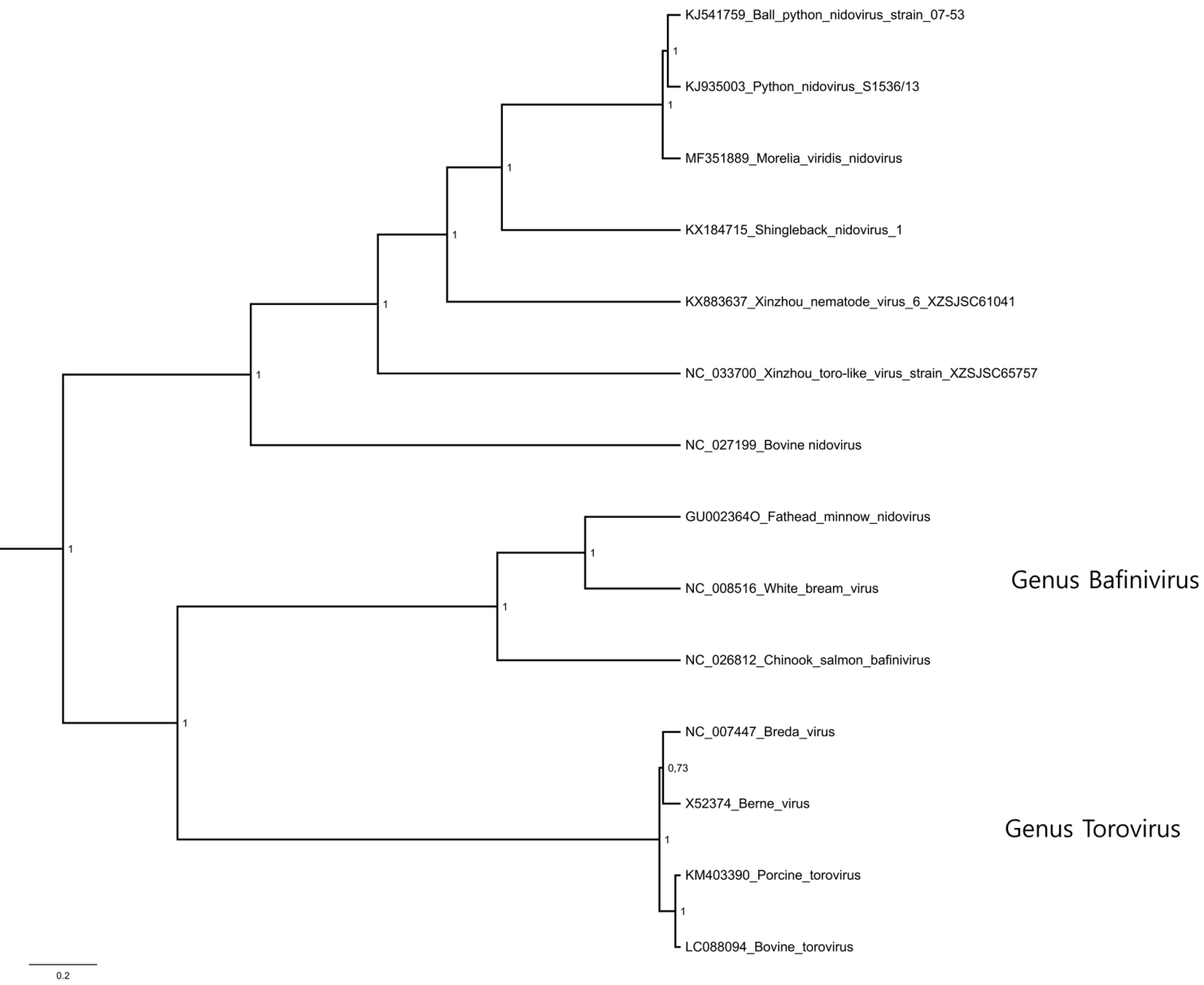
KJ541759_Ball_python_nidovirus_strain_07-53
KJ935003_Python_nidovirus_S1536/13
MF351889_Morelia_viridis_nidovirus
KX184715_Shingleback_nidovirus_1
KX883637_Xinzhou_nematode_virus_6_XZSJSC61041
NC_033700_Xinzhou_toro-like_virus_strain_XZSJSC65757
NC_027199_Bovine nidovirus
GU002364O_Fathead_minnow_nidovirus
NC_008516_White_bream_virus
NC_026812_Chinook_salmon_bafinivirus
NC_007447_Breda_virus
X52374_Berne_virus
KM403390_Porcine_torovirus
LC088094_Bovine_torovirus
0,73
1
0.2
Genus Bafinivirus
Genus Torovirus

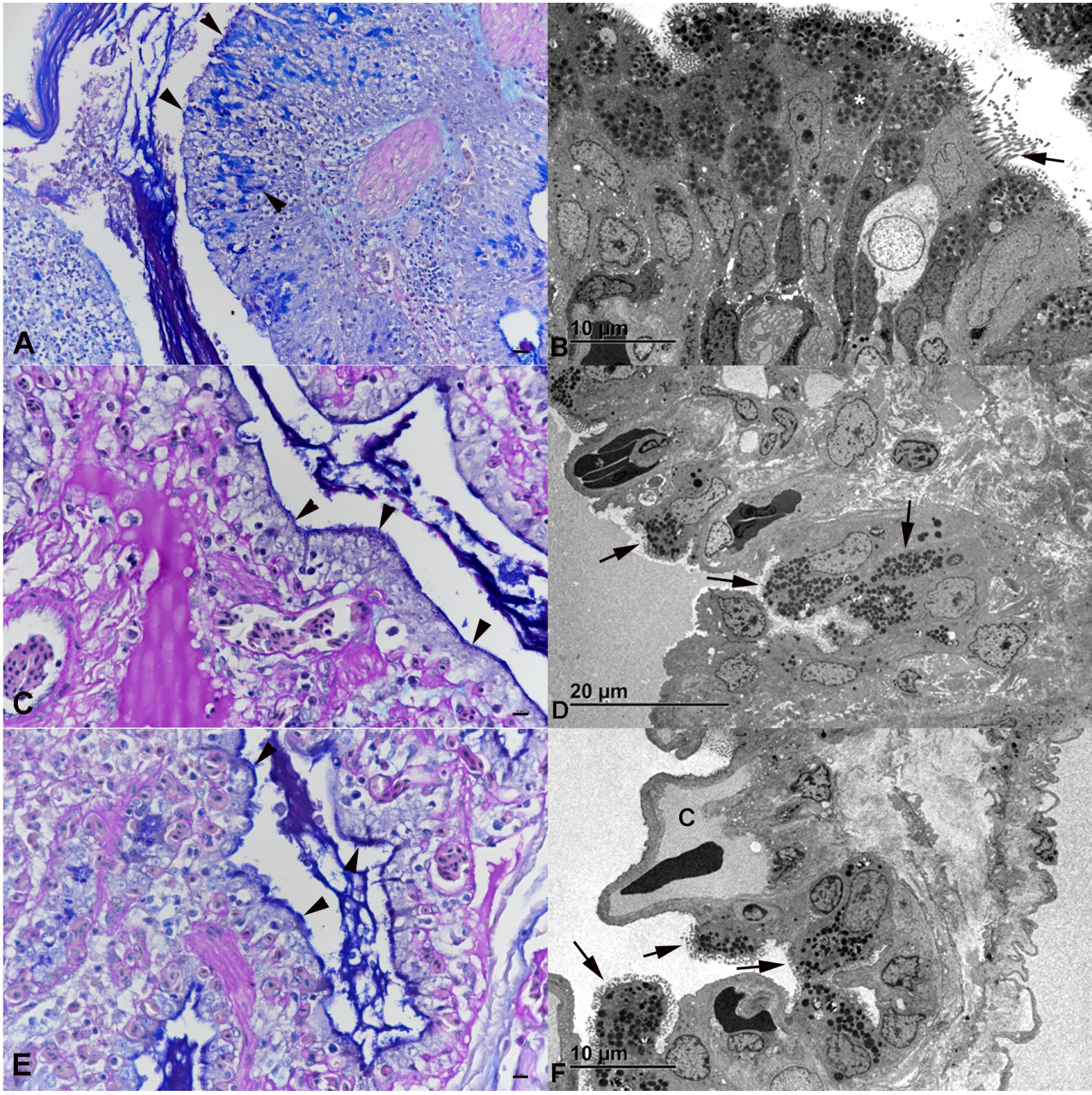
Region 1
Region 2
Region 3
A
B
10 µm
C
D
20 µm
E
C
F
10 µm

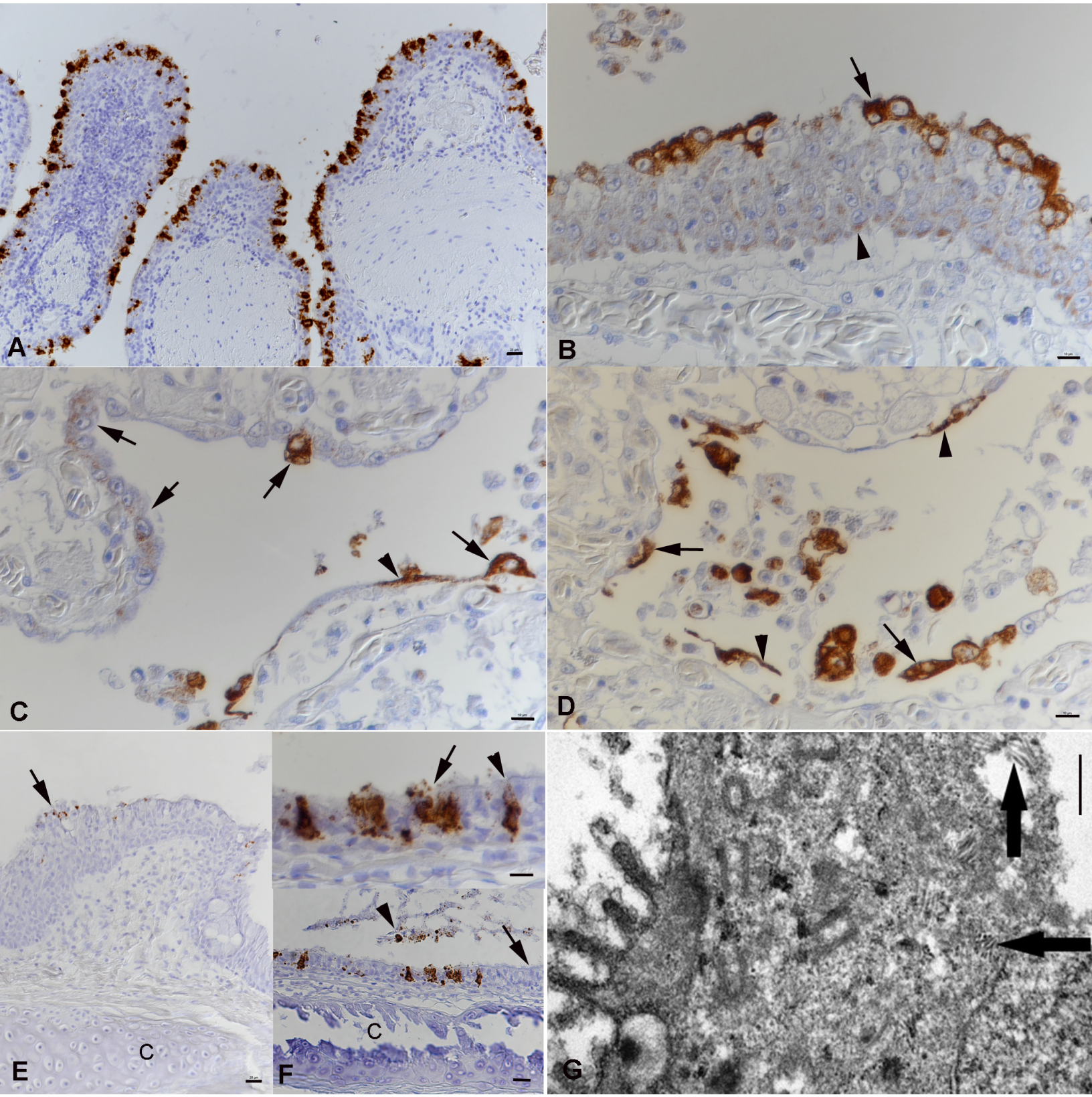
A
B
C
D
E
C
F
C
G

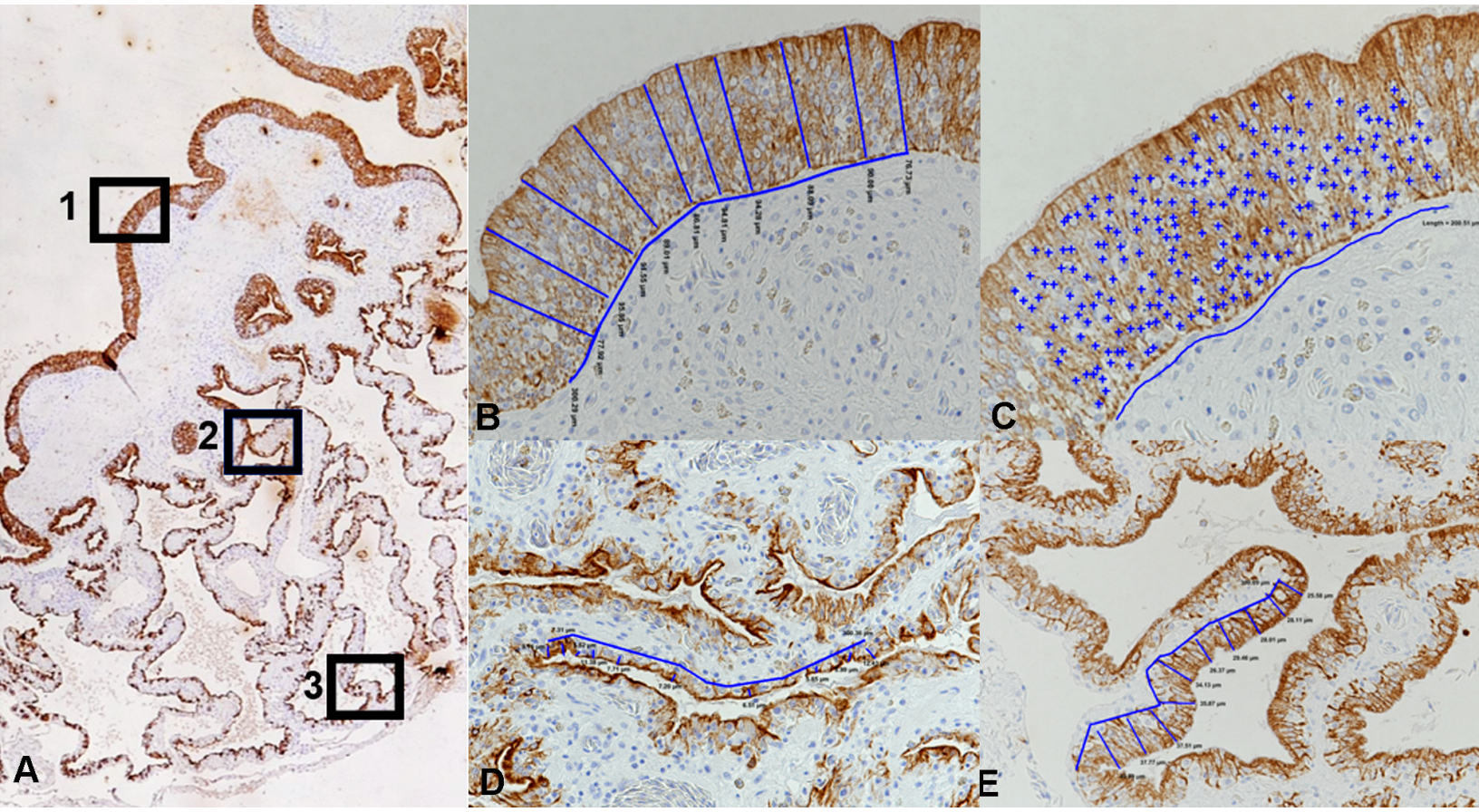
1
2
3
A
B
C
D
E

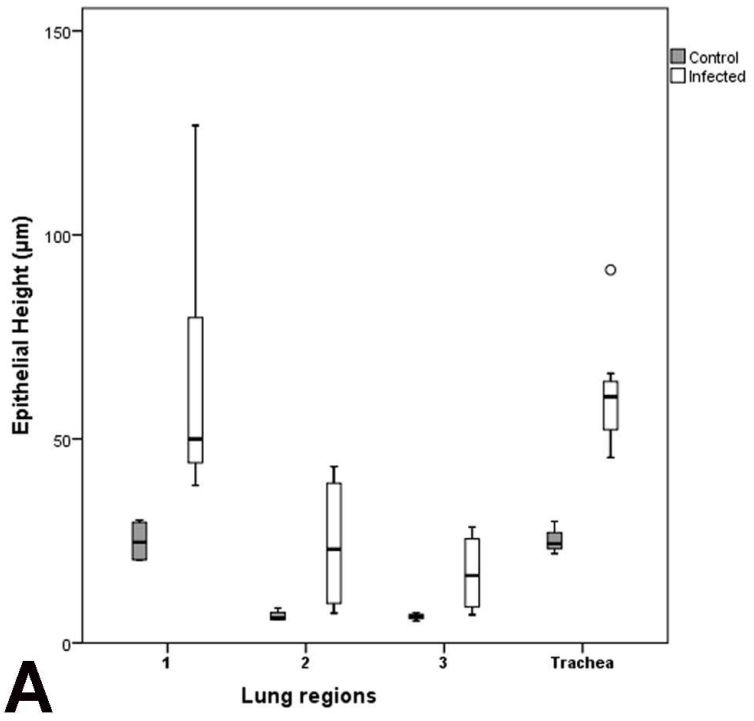
Epithelial Height (µm)
150
100
50
0
Control
Infected
1
2
3
Trachea
Lung regions

A

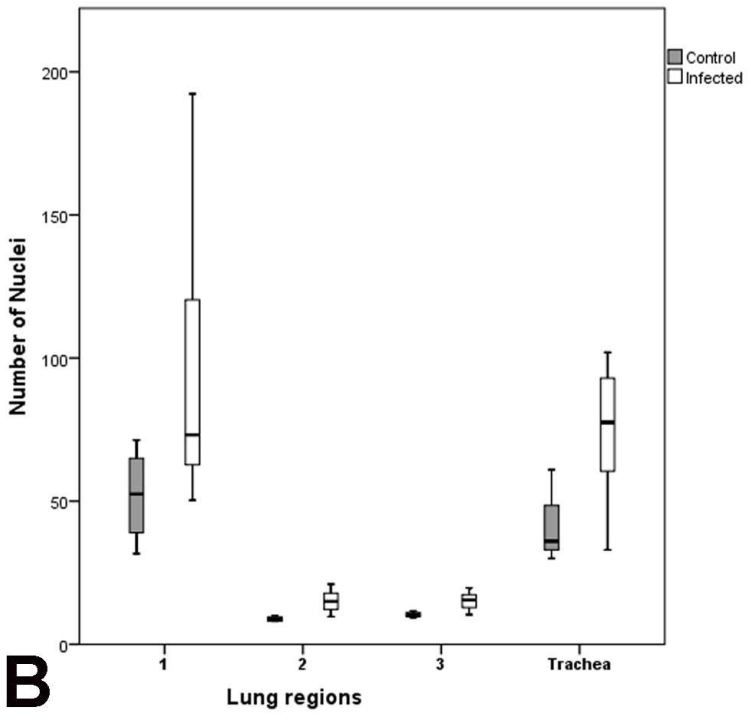
Number of Nuclei
200
150
100
50
0
Control
Infected
1
2
3
Trachea
Lung regions

B

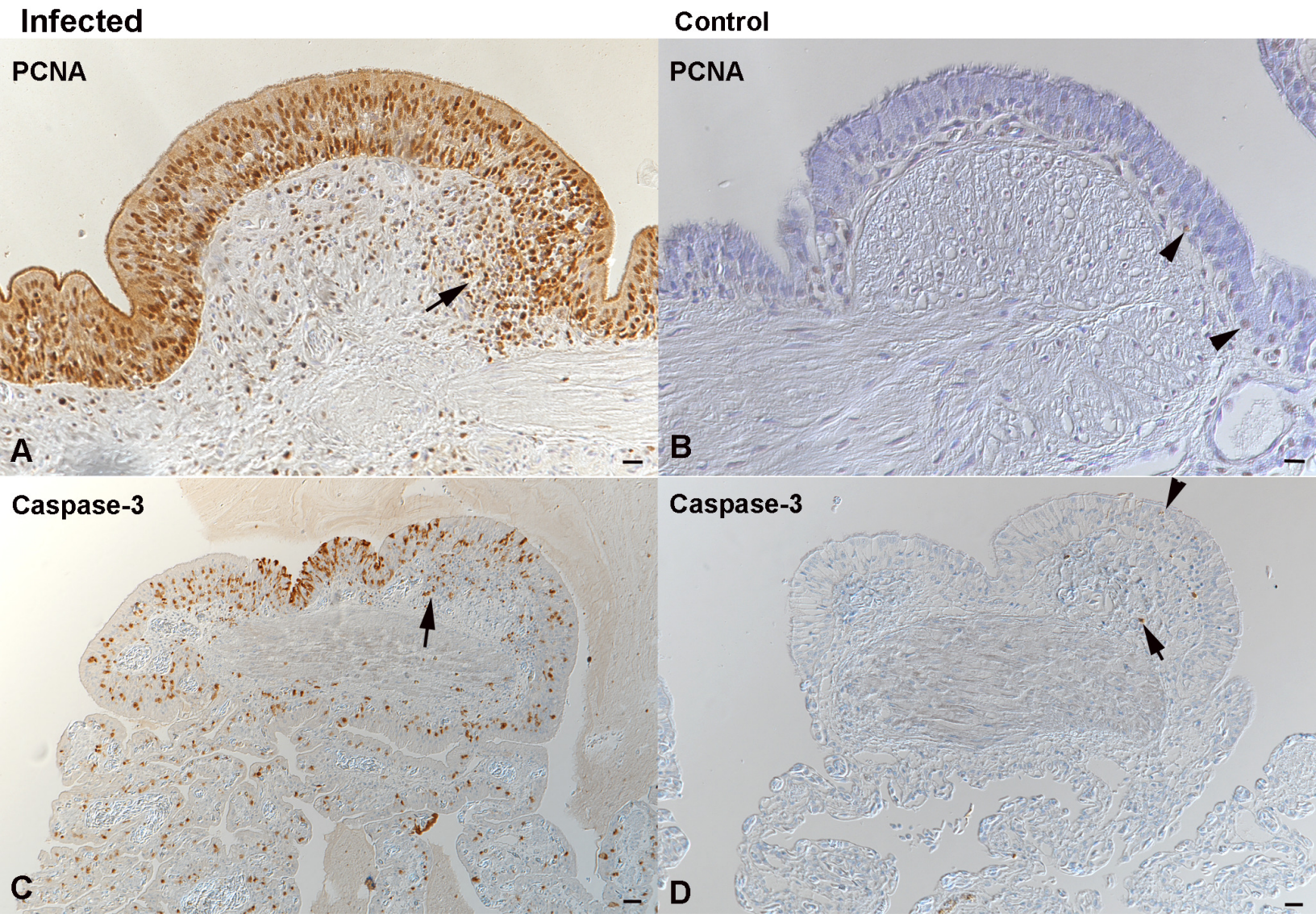
Infected
Control
PCNA
PCNA
A
B
Caspase-3
Caspase-3
C
D